

Artificial Intelligence Models for Digitized Operations and Maintenance of Large
Infrastructure Systems

by

Bala Sai Krishna Paladugu

A Dissertation Presented in Partial Fulfillment
of the Requirements for the Degree
Doctor of Philosophy

Approved June 2023 by the
Graduate Supervisory Committee:

David Grau, Chair
James Ernzen
Richard Standage

ARIZONA STATE UNIVERSITY

August 2023

ABSTRACT

Large-scale civil infrastructure systems are critical for the functioning and development of any society. However, these systems are often vulnerable to degradation and the effects of aging, necessitating consistent monitoring and maintenance. Current methods for infrastructure maintenance primarily rely on human intervention and need the implementation of advanced sensing and computing technologies in field operations and maintenance (O&M) tasks. This research aimed to address these gaps and provide novel contributions. Specifically, the objectives of this study were to leverage artificial intelligence models to enhance point cloud noise processing, to automate tree species detection using Mask R-CNN, and to integrate imagery data and LiDAR datasets for real-time terrain analysis. First, the study proposed leverages neural networks to eliminate unwanted noise from point cloud datasets, enhancing the accuracy and reliability of infrastructure data. Secondly, the research integrated Mask R-CNN into automated tree species detection. This component offers an efficient solution to identify and classify vegetation surrounding infrastructure, enabling infrastructure managers to devise proactive vegetation management strategies, thereby reducing risks associated with tree-related incidents. Lastly, the study fused image and LiDAR datasets to support real-time terrain analysis. This integrated approach provides a comprehensive understanding of terrain characteristics, allowing infrastructure managers to assess slope, elevation, and other relevant factors, facilitating proactive maintenance interventions and mitigating risks associated with erosion. These contributions collectively underscore the potential of artificial intelligence models in advancing the operations and maintenance practices of large civil infrastructure systems. By leveraging these models, infrastructure managers can

optimize decision-making processes, streamline maintenance efforts, and enhance critical infrastructure networks' overall resilience and sustainability.

DEDICATION

I dedicate this work to my parents, Purnachandra Prasad and Jayalalitha, and my brother, Manoj Kumar. Your unwavering faith in me and your boundless love and support has been the cornerstone of all my endeavors. I also dedicate this work to my wife, Niharika, whose patience, understanding, and companionship have been an invaluable source of comfort and encouragement through this journey. Lastly, a special dedication goes to my best friend, Avinash Reddy, who has been a constant ally, confidant, and source of inspiration. This accomplishment belongs as much to you all as it does to me.

ACKNOWLEDGMENTS

I express my deepest gratitude to my Ph.D. advisor, Dr. David Grau. His persistent support, wise guidance, and inspirational motivation were instrumental during my doctoral studies. His mentorship was academically enriching and greatly fostered my personal growth. My appreciation extends to my distinguished Ph.D. dissertation committee, Dr. James Erzen and Dr. Richard Standage. Their valuable suggestions broadened my research horizons and incited me to view my work from diverse perspectives.

In addition, I would like to convey my sincere gratitude to the Salt River Project (SRP, Tempe, Arizona) and the Ira A. Fulton School of Engineering for their collaborative efforts and financial support via project grants during my graduate studies. The support has been instrumental in facilitating this research. I'm greatly indebted to the entire team at SRP - Mr. Todd Rakstad, & Ms. Lori Jones. Their substantial support and assistance were key to the successful execution of this research.

TABLE OF CONTENTS

	Page
LIST OF TABLES	vii
LIST OF FIGURES	viii
CHAPTER	
1 INTRODUCTION	1
Impact of Ageing Infrastructure and Deficiencies On U.S. Economy and Citizens	2
Operations and Maintenance (O&M) of Civil Infrastructure Systems	4
Opportunity for Novel/Robust Analytical Algorithms.....	6
2 RESEARCH SCOPE AND OBJECTIVES	8
Research Hypothesis	8
Scope & Objectives	8
3 METHODOLOGY	10
4 LITERATURE REVIEW	13
State-of-Art O&M Activities	13
Noise Filtering	16
Terrain Analytics	20
Detection and Classification of Tree Species	24
5 DATA COLLECTION	28
Region of Interest (ROI).....	29
Geo-reference Points	30
Data Acquisition	30

CHAPTER	Page
Post-Processing.....	31
6 AUTOMATED NOISE FILTERING FROM HIGH REFLECTIVE ENVIRONMENTS	33
Noise Filtering Algorithm Framework	35
Validation.....	47
Limitations	57
7 TERRAIN ANALYTICS	58
Algorithm Framework for Terrain Analytics	60
Visualization	68
Limitations	70
8 TREE SPECIES DETECTION AND CLASSIFICATION	72
Mask R-CNN Architecture.....	73
Training, Validation, and Testing Datasets.....	75
Proof of Concept.....	78
Limitations	93
9 CONCLUSION	94
10 BROADER IMPACTS	97
11 INTELLECTUAL MERIT	99
REFERENCES	100

LIST OF TABLES

Table		Page
1	Pseudo Code for DBSCAN Clustering Algorithm.....	40
2	Pseudo Code for Supervised Neural Network for Noise Filtering	45
3	Noise Filtering Methods and Testing Environments.....	48
4	Results from Processing Two side Terrain Raw Point Cloud Dataset	49
5	Evaluation of Noise Filtering Algorithms on Low Noise Dataset.....	53
6	Evaluation of Noise Filtering Algorithms on Medium Noise Dataset	54
7	Evaluation of Noise Filtering Algorithms on Heavy Noise Dataset.....	56
8	Pseudo Algorithm for Fusing Camera Images with LiDAR Information	64
9	Area Under the Terrain Grade Heatmap.....	70
10	Pseudo Code for Mask R-CNN Implementation.....	77

LIST OF FIGURES

Figure		Page
1	Research Methodology	12
2	Noise in Civil Infrastructure Point Cloud	16
3	Region of Interest Canals Under Jurisdiction of SRP	29
4	Mobile Lidar Unit	31
5	Photographic Image of 3D Point Cloud.....	32
6	Noise in Raw Point Cloud Dataset.....	34
7	Type of Noise in Raw Point Cloud Dataset.....	36
8	Noise Filtering Algorithm Framework	36
9	Type of Datasets for Analytics.....	38
10	DBSCAN Clustering of Point Cloud Dataset.....	39
11	Data Clusters Post-Reflection Noise Processing	42
12	Processed Point Clouds Post-Noise Filtering	44
13	Training Loss Curve of Noise Filtering Neural Network Model.....	46
14	New Test Dataset.....	48
15	Low Surface Noise Dataset.....	52
16	Medium Surface Noise Dataset.....	54
17	Heavy Noise Dataset	55
18	Types of Road Crown Surface	58
19	Camera and LiDAR Data Fusion	62
20	Fused RGB LiDAR data on Camera Pixels.....	63
21	Computing Window for Data Frame	65

Figure	Page
22 SOTM Algorithm Framework	67
23 Visualization of Surface Grade Map Integrated with Fusion Dataset	69
24 Mask R-CNN Framework	73
25 Mask R-CNN Workflow	75
26 Tree Species Leveraged for Model Training	76
27 Model Prediction Sissoo Tree, Confidence = 77.6%	79
28 Model Prediction Sissoo Tree, Confidence = 84.9%	80
29 Model Prediction Sissoo Tree, Confidence = 97.3%	80
30 Model Prediction Sissoo Tree, Confidence = 97.0%	81
31 Model Prediction Sissoo Tree, confidence = 79.9%	81
32 Tree Species Dataset -Training Loss Curve	83
33 Tree Species Dataset -Training Bounding Box Loss Curve	84
34 Tree Species Dataset -Training Class Loss Curve.....	84
35 Tree Species Dataset -Training Mask Loss Curve	85
36 Tree Species Dataset -Training RPN BBox Loss.....	85
37 Tree Species Dataset -Training RPN Class Loss.....	86
38 Tree Species Dataset -Validation Loss	86
39 Tree Species Dataset -Validation BBox Loss.....	87
40 Tree Species Dataset -Validation Class Loss	87
41 Tree Species Dataset -Validation Mask Loss	88
42 Tree Species Dataset -Validation RPN BBox Loss.....	88

Figure		Page
43	Tree Species Dataset -Validation RPN Class Loss	89
44	Loss Curves for Tree Species Dataset	89
45	Accuracy on Testing Dataset – Mesquite Trees	91
46	Accuracy on Testing Dataset – Paloverde Trees	91
47	Accuracy on Testing Dataset – Palm Trees	92
48	Accuracy on Testing Dataset – Eucalyptus Trees	92
49	Accuracy on Testing Dataset – Sissoo Trees.....	93

CHAPTER 1

INTRODUCTION

Infrastructure is the backbone of the U.S. economy and necessary input to every economic output. The U.S. has a twenty-four trillion-dollar economy that relies on a vast infrastructure network, from transportation systems, water supply and treatment facilities, energy grids, and communication networks. According to the National Council of Public Works Improvement (NCPWI), a productive economy and quality of life rely on three essential elements: good transportation, supply of clean water, and safe disposal of wastes (NCPWI, 1998). Supporting NCPWI, the American Society of Civil Engineers (ASCE), in their civil infrastructure performance report card, clearly states that a nation with good and adequate civil infrastructure that meets the needs of the society can boost the nation's economy (ASCE, 2017):

- Business productivity,
- Gross domestic product (GDP),
- Employment,
- Personal income of households, and
- International competitiveness.

However, the U.S. built the most reliable transportation and water supply systems in the late 1950s. Since then, the U.S. population has grown by more than 100%, which makes these old infrastructure systems inadequate to fulfill the current requirements and inefficient in meeting the demands of society (NCPWI, 1998).

1.1 Impact of Ageing Infrastructure and Deficiencies on U.S. Economy And Citizens

The deteriorating condition of the U.S. infrastructure systems significantly affects U.S. economic growth and business productivity. According to ASCE, the U.S. infrastructure received a grade of C- on their 2021 Infrastructure Report Card, indicating that it requires significant investment to maintain and improve (ASCE, 2021). The ASCE estimated that the cost of deferred maintenance and needed upgrades to the U.S. infrastructure systems will reach \$5.6 trillion, i.e., 24% of GDP by 2029. This includes transportation, water and wastewater systems, energy/ power system grids, and other critical infrastructure investments. According to the previous estimations of ASCE, the cumulative cost of inadequate infrastructure systems has cost the U.S. economy more than \$3.1 trillion in GDP and \$1.1 trillion in lost business trade between the years 2012-2020 (ASCE, 2021). This includes lost productivity, increased transportation costs, and decreased competitiveness in the global marketplace. Further, the revised ASCE estimates predict that the continued underinvestment in infrastructure at current rates would cost \$10 trillion in GDP, 3.5 million lost jobs, and cost \$2.24 trillion in exports by the year 2039 (ASCE Failure to Act, 2021).

In addition to the economic loss, the deteriorating infrastructure systems have cost U.S. citizens billions of dollars and time. According to the study report on the deficiencies of the U.S. transportation systems, citizens have lost 69 billion hours of productive business time to traffic delays (ASCE, 2016; FSWH, 2019). Further, the congested traffic routes have cost \$160 billion in wasted fuel (ASCE, 2016; FSWH, 2019). Also, the delays caused due to deficient infrastructure and avoided trips have cost implications of \$35 billion to the

U.S. economy each year (ASCE, 2021). Adding to it, the deteriorating conditions of roads have forced motorists to spend \$130 billion each year on extra vehicle repairs and operating costs (ASCE, 2021). In 2016, the ASCE predicted that the infrastructure systems' deficiencies may cost each household \$3400 in disposable income each year by 2025 (ASCE Failure to Act, 2016). However, the ASCE also estimated this loss would rise to \$5100 for each household in the United States by 2040 (ASCE Failure to Act, 2016).

Furthermore, the failure of these civil infrastructure systems has negative consequences for public safety and significant economic loss. A few examples of such failures are as follows:

- **Minneapolis Bridge Collapse:** The 2007 collapse of the Mississippi River bridge resulted in 13 deaths and 145 injuries. The collapse cost is estimated to be between \$250 million and \$300 million. (MacDonald & MacDonald, 2012)
- **The Flint water crisis:** The failure of infrastructure in Flint, Michigan, led to the contamination of the city's water supply with lead, resulting in health problems for residents. The estimated cost of the crisis is over \$400 million. (EPA, 2018)
- **The Los Angeles Water Break:** In 2014, a water main break in Los Angeles, California, caused flooding and damage to several homes and businesses. The cost of repairs and compensation to affected parties was estimated to be \$20 million. (LADWP, 2014)
- **The New York City blackout of 2003:** The infrastructure failure in the form of an electrical grid failure resulted in a widespread blackout affecting millions of residents, with an estimated cost of \$6 billion. (U.S. -Canada PSOTF, 2004)

To avoid such catastrophic failures, there is a significant opportunity to improve the current state-of-repair by optimizing the timely operations and maintenance procedures through leveraging innovative technologies (WEF, 2014).

1.2 Operations and Maintenance (O&M) of Civil Infrastructure Systems

Operations and maintenance (O&M) are the post-construction activities performed on the civil infrastructure systems to maintain a good repair state. The primary goal of performing O&M activities is to maintain accurate, updated, and reliable data on civil infrastructure, including physical characteristics (i.e., structural components of the infrastructure) and performance characteristics (i.e., changes on the infrastructure due to movement of traffic and weather conditions). O&M involves a wide range of activities such as (WEF, 2014):

- Inspection and data collection
- Condition assessment
- Performance evaluation
- Prediction of future performance
- Planning, prioritizing maintenance and repair
- Evaluating alternative technical solutions and economic policies

Large and aging civil infrastructure systems in the U.S. create greater pressure on concerned authorities to pursue O&M activities regularly. However, most O&M activities on civil infrastructure are carried out manually through visual inspections. Thus, optimizing O&M activities is a perennial problem that often delays O&M decisions. The

major challenges and limitations of carrying out O&M activities are as follows (WEF, 2014):

- O&M requires high-quality and precise information on infrastructure assets for decision-making on maintenance/repair activities. Due to the geographic spread of civil infrastructure over extensive areas, it is difficult to extract information from inaccessible and isolated rural areas.
- Implementing a proper maintenance strategy over a longer period for civil infrastructure assets is a complex and labor-intensive approach; it requires continuous monitoring and training, which takes a large amount of productive time.
- Civil infrastructure systems are inherently large and complex, composed of diverse materials and elements. Deterioration in civil structures is characterized by cracks, deflections, and corrosion caused by various factors such as environmental parameters, load incurred, and natural disasters. Integrating these complex parameters into a monitoring system is challenging.
- O&M is a multi-disciplinary process that involves many interdependent operations that need management in a coordinated manner. The lack of an integrated computerized tool makes it impossible to communicate and maintain infrastructure condition status effectively.
- Furthermore, O&M of civil infrastructure systems is a knowledge-intensive process that requires accessing and managing many knowledgeable resources. Relying on manual inspection procedures often results in slow information extraction, which leads to uninformed and delayed decisions.

However, technological innovations, particularly in sensor technology and active remote sensing, have significantly improved large civil infrastructure systems' operation and maintenance (O&M). Advancements in sensors and radio-frequency devices, such as strain gauges, accelerometers, and RFID tags, have enhanced safety, efficiency, and reliability by enabling real-time data collection and condition monitoring (Ansari, 2007; Stajano, 2010; Johnson et al., 2015; Smith & Brown, 2016; Williams, 2017). LiDAR, an advanced active remote sensing technology, offers a non-invasive alternative for acquiring real-time infrastructure data, allowing the creation of detailed 3D models to support performance analytics and more effective O&M strategies (Chen, 2007; Gupta & Way, 2010; Wu et al., 2021). LiDAR has been employed in various projects, including transportation, building and construction, water grid, and power grid infrastructure, with researchers developing computing algorithms to extract valuable information from 3D digitized models, automating data extraction and minimizing implementation costs and safety concerns (Qiao et al., 2021; Wu et al., 2020; Geng et al., 2022; Chu et al., 2022).

1.3 Opportunity for Novel/Robust Analytical Algorithms.

Despite the successful research efforts, the research gap in sensing and digitization of infrastructure systems for O&M tasks can be attributed to various aspects that require further exploration and development, particularly in handling sensor data to support O&M activities. Several limitations in sensor data processing algorithms persist when computing datasets from multiple sources. Variability in data quality, resolution, format, and accuracy is one of the major limitations affecting the performance of algorithms. For example, Point cloud data generated using different sensors/platforms, i.e., airborne method or terrestrial

method, have different point cloud densities, spatial resolution, and noise levels compared to point cloud data from the mobile mapping method, which affects the efficiency of algorithms to extract features and measurements.

Furthermore, the ability to process sensing data in various environmental conditions is critical for the successful implementation of O&M tasks. Research on adaptive algorithms that can account for varying environmental conditions during data acquisition is essential for improving the efficiency of sensor data processing. Standardizing data processing workflows and software tools will also greatly benefit the handling of O&M activities in civil infrastructure systems.

However, as the adoption of sensor technologies in civil infrastructure asset digitization is expected to grow in the coming years, there is a significant opportunity to address the shortcomings of the data processing tools by developing more robust and adaptive algorithms. Researchers and engineers can enhance infrastructure digitization and enable efficient automated information extraction and monitoring of analytical models that handle complex datasets and environments. This would ultimately contribute to better management of infrastructure assets and more effective and efficient handling of required O&M activities.

CHAPTER 2

RESEARCH SCOPE AND OBJECTIVES

2.1 Research Hypothesis

The development of novel analytical models with rich contextual information leveraging machine learning/ deep learning techniques promises to improve the ability to operate and maintain infrastructure systems that spread over large geographical domains.

2.2 Scope & Objectives

The scope of this research focuses on investigating, exploring, and developing analytical models, leveraging deep learning techniques to automate feature extraction from point cloud imagery data from highly reflective noisy environments acquired through mobile mapping of large civil embankment infrastructure systems. Even though the scope of this research focuses on infrastructure systems spreading over large areas, such as power transmission and distribution, roads and highways, or open water distribution, the methods could apply to other infrastructures and built assets. The study involves LiDAR data with physical features like trees, powerline cables, transmission poles, walls, fences, noise, soil terrain, etc. The analytical models are trained to identify and extract features such as noise, digital terrain, and tree classification. The proposed analytical models are trained on a combination of point cloud and imagery datasets, and the performance is validated compared to the traditional algorithms. The objectives of the study are as follows:

- Objective 1: Explore novel and robust supervised machine-learning analytical algorithms for noise filtering that can effectively distinguish noise generated from complex real-world environments.

- Objective 2: Explore the ability of robust analytical learning algorithms to support real-time terrain analytics of bare earth terrains by adopting data fusion between high-resolution point cloud and street-level imagery data.
- Objective 3: Investigate the ability of learning algorithms to extract tree specimens and classify tree species from street-level data containing complex contextual information.
- Objective 4: Prove the efficiency and validity of the proposed models and algorithms.

CHAPTER 3

METHODOLOGY

The methodology employed in this study involves leveraging artificial intelligence models to address the challenges associated with the operations and maintenance of aging large civil infrastructure. The research aims to develop innovative approaches that leverage the capabilities of neural networks, Mask R-CNN, and the fusion of image and LiDAR datasets to support infrastructure management efforts.

To achieve the first objective, a point cloud noise processing methodology will be developed using neural networks. This methodology will involve training a neural network model using a labeled dataset of infrastructure point clouds. The trained model will then be employed to process new point cloud data, removing noise and enhancing the accuracy and reliability of the infrastructure dataset.

The second objective is to implement an automated tree species detection method using Mask R-CNN. The Mask R-CNN algorithm will be trained on a dataset containing annotated images of various tree species. The trained model will be used to detect and classify tree species in the vicinity of the infrastructure, aiding in vegetation management and ensuring the safety and longevity of the infrastructure.

A real-time terrain analysis will be performed by fusing images and LiDAR datasets to accomplish the third objective. The image and LiDAR data will be processed and integrated to analyze terrain characteristics such as slope, elevation, and potential hazards. This analysis will provide infrastructure managers with timely insights for proactive decision-making and targeted maintenance interventions.

By employing these methodologies, this research seeks to contribute to the field of infrastructure management by leveraging artificial intelligence models to support operations and maintenance efforts for large civil infrastructure systems. The outcomes of this study will provide valuable insights into the effectiveness of these approaches and their potential to ensure that critical infrastructure systems are sustained good state of repair. Figure 1. illustrates the research methodology of this research study.

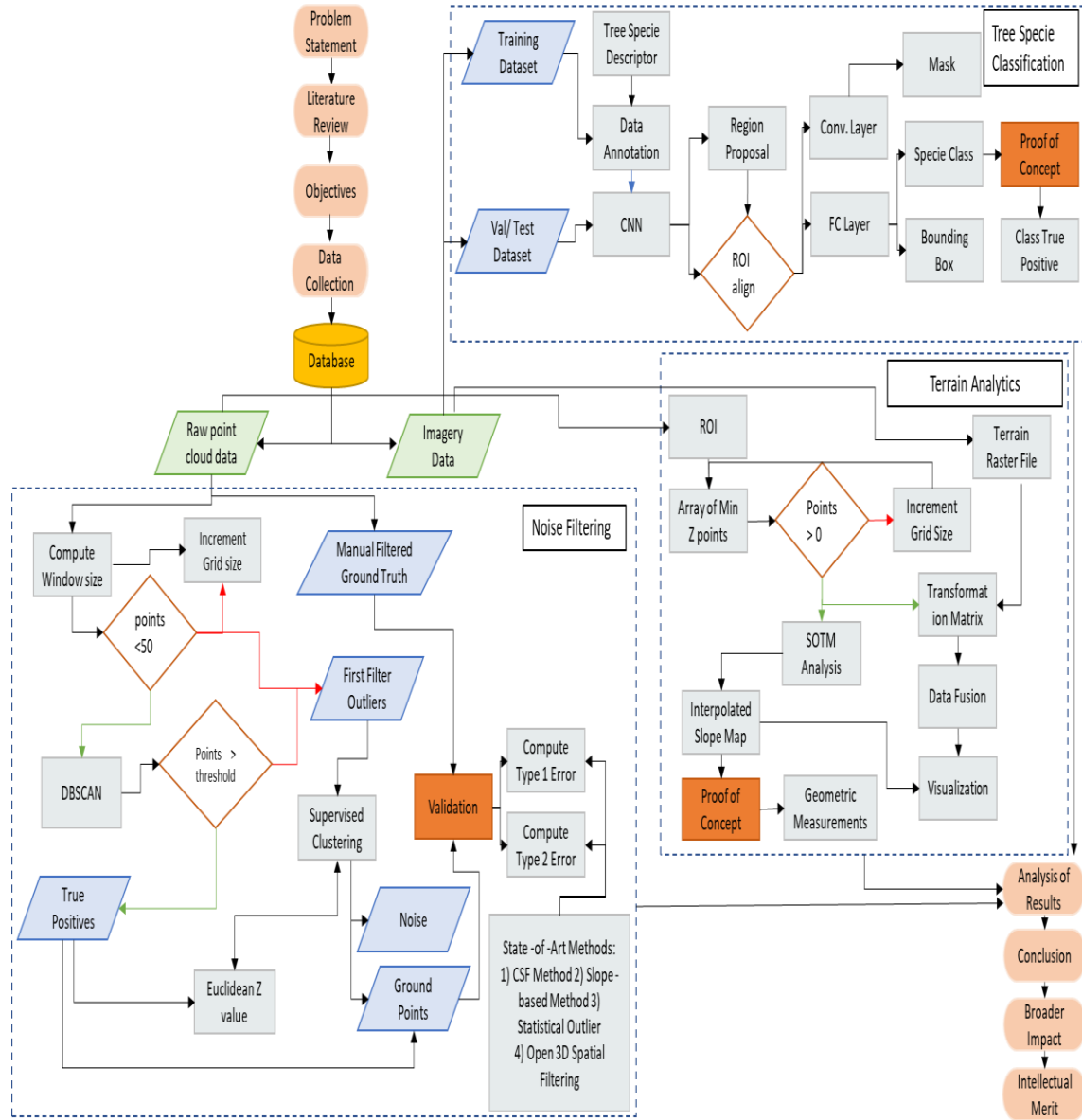


Figure 1. Research Methodology

CHAPTER 4

LITERATURE REVIEW

This section details a comprehensive literature review summarizing related research for processing remote sensing information from a digitized civil infrastructure system to support strategic O&M activities. The literature review is structured into four parts to provide a holistic understanding of the research area. The first part provides an overview of the current O&M activities through digitizing civil infrastructure systems and highlights the challenges of feature extraction algorithms. The second part discusses the various noise delineation methods and their limitations, detailing the challenges of accurately filtering noise from point cloud datasets. The third part examines the state-of-the-art techniques for analyzing infrastructure terrain and, highlighting the shortcomings, emphasizes the need for real-time terrain analysis. Finally, the fourth part explores deep learning-based image classification models for tree species detection and highlights the limitations, including their dependence on large and diverse datasets.

4.1 State-of-Art O&M Activities

LiDAR has become more popular in recent years for its ability to capture high-resolution 3D data at high speed from large areas. LiDAR sensor-generated point cloud data provides access to a wide range of infrastructure asset information, including object features, digital terrains, vegetation, boundaries, encroachments, etc. This has enabled O&M activities to be carried out more efficiently, cost-effectively, and accurately compared to the traditional manual methods, which are labor-intensive, time-consuming, and costly. Many research studies have highlighted the benefits of using digitized infrastructure assets for O&M

activities in building infrastructures, urban landscapes, and other large-scale infrastructures, including roads, bridges, embankments, etc. The following paragraph summarizes the previous research efforts in large civil infrastructure systems.

4.1.1 Large Civil Infrastructure Systems

Lidar-based analytical models are increasingly applied in large civil infrastructure projects for damage assessment, flood mapping, and corrosion analysis to maintain and manage structural health. Relevant studies in optimizing operation and maintenance include UAV-based inspection on bridges by Khaloo et al. (2018), UAVs for damage inspection of bridges by Lovelace and Zink (2015), flood segmentation and depth identification using lidar data by Cai et al. (2007), and leak detection in canal systems using airborne multispectral data by Huang et al. (2009) and Arshad et al. (2014). Yang et al. (2014) proposed an automatic road marking extraction method from MLS point clouds. Additionally, researchers have used airborne lidar technology to study land surface conditions, analyze land cover patterns, and classify objects (Hecht et al., 2008; Huang et al., 2013; Giridharan et al., 2004; Coren & Sterzai, 2006; Höfle & Pfeifer, 2007; Kakon et al., 2009; Kotthaus & Grimmond 2014; Zhou & Troy, 2008; Zhou et al., 2009; Zhou, 2013; Samal & Gedam, 2015; Zhang et al., 2008). Numerous studies have applied an object-oriented approach using lidar data fused with image analytics, which has shown better results in classifying building footprint, pavement, bare soil, fine-textured vegetation, and coarse-textured vegetation (Zhou & Troy, 2008; Zhou et al., 2009; Zhou, 2013; Samal & Gedam, 2015). Overall, these studies highlight the potential of lidar technology in contributing to the optimization of O&M activities in large civil infrastructure projects,

enabling more efficient and effective maintenance and management of these critical systems.

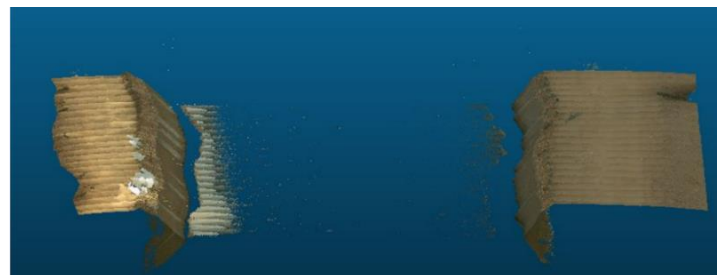
4.1.2 General Limitations of Current Analytical Methods

The accuracy and efficiency of feature extraction algorithms are challenges for digitizing civil infrastructure assets for O&M activities. Many researchers have emphasized that the performance of point cloud processing algorithms is affected by many factors, including variability in data quality, resolution, format, and accuracy of point cloud datasets (Wang et al., 2017; Xiao et al., 2017; Zhang et al., 2017; Sithole & Vosselman, 2004; Vosselman & Maas, 2010; Rottensteiner et al., 2013). Also, Lei et al. (2020) and Wang et al. (2020) reported that Integrating data from various sources can be computationally demanding. They may result in inconsistencies and errors while processing large volumes of data. Additionally, Li et al. (2020) point out that the lack of standardization in data processing tools and hardware hampers the comparability of results across different studies. For instance, Borkar et al. (2020) found inaccuracies in the structural analysis due to difficulties in extracting meaningful information from point cloud data for concrete infrastructure. Furthermore, Du et al. (2018) highlighted the challenges of integrating data from multiple sources for road infrastructure management, leading to inconsistencies in data and making it challenging to make informed decisions about maintenance and repair. There is a significant opportunity to improve the accuracy and efficiency of processing tools for large point cloud datasets of civil infrastructure from complex reflective environments. The following paragraphs provide an overview of research studies on point cloud processing

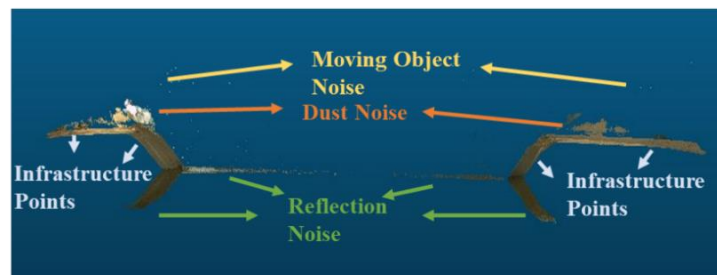
analytical models, including noise filtering, real-time terrain analysis, and tree species classification from the point cloud and imagery datasets.

4.2 Noise Filtering

Point cloud datasets obtained through mobile LiDAR scanning are susceptible to noise, which may be caused by various factors such as the weather condition and continuous data collection process from an on-ground movable vehicle (Li et al., 2019). Researchers used the terms "outliers" and "noise" interchangeably. Salgado et al. (2009) and Bastani et al. (2019) have defined noise as misleading points in the dataset generated due to dust because of vehicle speed, reflection from surrounding water bodies and moving objects such as vehicles, humans, and birds. The presence of noise in point cloud datasets can negatively impact the accuracy and reliability of the results, making it challenging to extract feature extraction information for various applications such as civil infrastructures.



a) Raw Point Cloud of Infrastructure Surface



b) Distinguished Noise and Infrastructure Points

Figure 2. Noise in Civil Infrastructure Point Cloud

4.2.1 State-of-Art Noise Filtering Methods

The first step in processing point cloud data is to segment it into infrastructure ground points and non-ground points. However, due to the lack of geometrical similarities and topography between ground and non-ground features, filtering point clouds has proven challenging (Sithole & Vosselman, 2004). Therefore, various filtering methods have been explored to filter noise features in large lidar point clouds, which are typically divided into three categories: slope-based, linear prediction-based, and surface-based methods (Sithole & Vosselman, 2004; Liu, 2008; Zhang & Witman, 2005; Bartels & Wei, 2010).

Slope-based algorithms are successful in point cloud datasets with flat areas, but their accuracy decreases in steep terrains (Vosselman, 2000; Sithole, 2001; Shan & Sampath, 2005; Wang & Tseng, 2010). Shan and Aparajithan (2005) improved the slope-based filtering algorithm's accuracy by calculating the slopes between neighbor points along a single scan line in a specified direction. Meng et al. (2009) extended the algorithm's application to multidirectional scan lines. On the other hand, linear prediction-based methods have been proven inefficient in preserving terrain details and tend to misclassify minute objects (Sithole & Vosselman, 2004; Liu, 2008), despite various threshold calibration methods being used, such as direction filters and adaptive filters (Wang & Tseng, 2010; Sithole, 2001; Susaki, 2012).

Morphological filters effectively preserve terrain details and remove small objects in steep terrains. However, selecting the right processing window size is crucial (Kilian, 1996; Lohmann et al., 2000; Zhang et al., 2003; Sithole & Vosselman, 2005; Zhang & Witman, 2005; Chen et al., 2007). Small processing windows remove small objects, leaving large

objects like buildings untouched, while large processing windows flatten terrain details. Kilian et al. (1996) proposed a solution to this issue by applying morphological filtering with gradually increasing window size and assigning weights to each point based on the processing window size by which it is recognized as a ground point. The terrain surface is then estimated using the weighted points' surface approximation. Similarly, Zhang et al. (2003) proposed a progressive morphological filtering method for constant inclinations, but the assumption of constant slope may lead to poor surface results. Additionally, a few other mathematical morphological-based filtering algorithms include morphological reconstruction (Arefi & Hahn, 2005), full-waveform methods (Mucke et al., 2010), and repetitive interpolation (Kobler et al., 2007). However, accuracy depends on the processing window size parameter, which requires prior knowledge of the study area.

Surface-based methods gradually approximate the ground surface by iteratively selecting ground measurements from the original dataset (Axelsson, 2000). Zhang and Lin (2013) improved accuracy by embedding smoothness-constrained segmentation. However, the results are inconsistent with the steeper slope surfaces.

In recent times, Zhang et al. (2016) proposed an advanced cloth simulation model (CSF) to extract terrain surfaces from the lidar point clouds from airborne datasets. Unlike the other filtering algorithms with complicated parameter setups, the CSF algorithm uses simple integer and Boolean parameters for mesh grid and iteration setups. The algorithm first inverts the point cloud dataset and simulates rigid cloth covering the inverted surface. The noise is identified and filtered by analyzing the surface interactions of point clouds with the cloth grid surface. However, this filtering technique's results were insignificant

while processing high-resolution point cloud datasets from reflective environments, misinterpreting vertical slope as noise and failing to filter noise generated from surrounding reflective water bodies.

4.2.2 Limitations of Noise Filtering Methods

A major limitation of previous studies is the challenge of processing heavy noise point cloud datasets. Current noise filtering methods, such as morphological filters, linear prediction-based methods, and surface-based methods, have been proposed to filter out noise from point cloud datasets. However, these methods face limitations related to data density and reflective environments, which can affect the accuracy of ground-truth information in the point cloud datasets.

For instance, morphological filters require appropriate threshold and window size selection for processing. At the same time, linear prediction-based and surface-based methods are inefficient in classifying and processing noise around steep vertical slopes. Furthermore, while these previous algorithms have effectively filtered noise from horizontal planar surfaces from point cloud datasets acquired through airborne methods, they were not accurate enough in filtering noise generated due to reflection and often miss-classify steep vertical slope points as noise.

Thereby, this research explores novel and robust supervised machine-learning analytical algorithms for noise filtering that can effectively distinguish noise generated from complex real-world environments (Objective 1).

4.3 Terrain Analytics

Large infrastructure networks often extend over vast areas, encompassing terrain types such as asphalt, concrete, and earthen soil roads. These diverse terrains face several challenges due to factors such as uncontrolled water discharge, traffic load, and environmental conditions. Effective management and maintenance of these terrains are crucial to ensure the longevity and functionality of the infrastructure.

Uncontrolled water discharge, often from rain, can lead to standing water penetrating road surfaces, creating potholes or puddles. This infiltration weakens the terrain surface and base, causing material loss and making the infrastructure more susceptible to erosion. Additionally, due to moving traffic, unpaved terrain surfaces may experience abrasion, compaction, and displacement of surface material. Over time, the combined effects of traffic and complex environmental conditions can wash out surface aggregates, emphasizing the need for regular profile grading and maintenance of infrastructure terrains. Notably, unpaved terrains require two to three times more maintenance than paved roads, as they do not possess the same resistance to water infiltration as asphalt or concrete roads. To address these challenges, many researchers have explored advanced computing models to analyze terrain surface grades (slopes). The following sections of this paper will provide a detailed overview of such research efforts.

4.3.1 State-of-Art Terrain Assessment Methods

Lidar data has emerged as a valuable source of information for terrain analysis, enabling the assessment of slope grade, cross-slope, and erosion. By processing this data into Digital Elevation Models (DEMs), the surface elevation of the earth's terrain can be determined,

facilitating the calculation of terrain parameters such as slope and aspect. Traditional methods of determining slope grade relied on manual measurements and topographic maps, which were time-consuming, expensive, and limited by low resolution.

Terrain profile grade is an essential feature impacting natural and human-made systems. For example, it plays a role in transportation by determining sight distance on vertical curves (Souleyrette et al., 2003), water distribution embankment networks by controlling and preventing uncontrolled water discharges (Paladugu et al., 2020; Paladugu & Grau, 2018), and agriculture by identifying areas prone to erosion, which affects soil fertility and crop productivity.

Researchers have used lidar data to create terrain profile maps, employing mathematical algorithms such as the Savitzky-Golay filter (1964), Loess method (1979), Horn algorithm (1981), Zevenbergen and Thorne algorithm (1996), and Slangen algorithm (1996) to calculate terrain grade profiles. However, these algorithms vary in accuracy and computational efficiency. Visualization techniques for terrain grade profile maps have also been developed, including color coding and shading. Machine learning techniques, like support vector machine (SVM) algorithms, have been utilized to train models for distinguishing between grade categories (Liu et al., 2018). Despite these advancements, there are limitations, such as a lack of semantic understanding of dynamic terrain scenes, which can result in inaccurate measurements (Chen et al., 2019).

Recent advances in real-time terrain analysis methods, particularly those employing deep learning techniques, have demonstrated promising results in applications like erosion trend estimation and terrain classification (Zheng et al., 2018). These real-time methods fuse

datasets, such as imagery and point cloud data, to provide rich contextual information, including color, texture, semantic information, and precise measurements of distances and elevations (Ghaffarian et al., 2019). Data fusion has been shown to improve terrain analysis results by addressing the limitations of geometric methods. Real-time methods fusing image and LiDAR datasets have emerged as a promising approach for terrain analysis, addressing the limitations of traditional geometric methods and providing richer contextual information. These methods leverage information from both datasets, enhancing the understanding of various terrain types and environmental conditions. For example, in the context of terrain analysis, recent studies have utilized deep learning techniques to combine multispectral images and LiDAR-derived elevation data for improved terrain classification and segmentation (Yang et al., 2020). The method has demonstrated proficiency in accurately classifying distinct terrain features, including topographical attributes, slopes, and vegetation. These are crucial for various applications such as monitoring erosion, evaluating hazards, and planning land use. Another notable development is using 3D object detection frameworks, such as VoxelNet, which integrates image and LiDAR data to efficiently learn local spatial features and context information for robust object detection in complex urban environments (Zhou et al., 2018). These methods have also been applied to infrastructure condition assessment, such as automated bridge inspection using fused images and LiDAR data to detect and analyze bridge defects (Ye et al., 2019). This approach offers a more detailed and robust representation of surface features and structures, allowing for precise assessment of surface morphology and changes over time. Moreover, image and LiDAR data fusion have been applied in monitoring natural calamities, such as

landslides, soil erosion, and vegetation dynamics, providing valuable insights for environmental management and conservation (Qin et al., 2020).

4.3.2 Limitations of Real-Time Terrain Analysis

Change detection from terrain surface and estimation of erosion trends leveraging point cloud datasets has been a highly effective tool for terrain morphology assessment. Unlike paved terrains, unpaved terrain deteriorates faster due to traffic flow and complex environmental conditions, such as heavy rains and floods, leading to infrastructure failure. However, geometric methods can successfully generate the terrain morphology and erosion trends from point cloud datasets, including Triangulated Irregular Network (TIN), Digital Elevation Model (DEM), Savitzky-Golay filter, Loess method, support vector machines, etc. However, these geometric methods lack a semantic understanding of dynamic unpaved terrain scenes and are sensitive to noise, and outliers result in inaccurate measurements while processing raw point cloud datasets. The advances in multiple data fusion technologies provide an opportunity to address these limitations through real-time analytics by leveraging imagery and point cloud datasets. Fusion of multiple datasets, such as imagery and point cloud datasets processed with deep learning (DL) algorithms, provides access to rich contextual information, such as color, texture, and semantic information, and precise measurement of distances and elevations.

Recent research studies on paved terrains using real-time methods have reported varying levels of accuracy, ranging from 80% to 95%. However, these research methods were developed with learning algorithms trained on contextual information from terrain scenes captured from an aerial view. Although a few studies have employed street-level data

fusion methods, the primary focus has been object detection rather than terrain morphology assessment. Consequently, these methods may not be directly adaptable for unpaved terrain datasets due to factors such as undefined boundaries, differences in perspective views and contextual information training, and varying data fusion alignment. Moreover, previous studies have faced computational limitations resulting from misalignment during data fusion and noise, leading to errors of 5%-20% in terrain classification. Addressing these limitations will be crucial in advancing real-time terrain analysis methods for unpaved surfaces with street-level data.

Thereby, this research explores the ability of robust analytical learning algorithms to support real-time terrain analytics of unpaved terrains by adopting data fusion between the high-resolution point cloud and street-level imagery data from heavy noise reflective environment (Objective 2).

4.4 Detection And Classification of Tree Species

Growth of vegetation along the power line infrastructure corridors may result in tree limbs' intervention with power conductors, causing a short circuit, power blackout, or even fire. Control of vegetation growth requires regular inspections and a deep understanding of tree species and their growth rate. Different tree species have different textural and spectral characteristics.

The emergence of Deep Learning (DL) architectures such as Convolutional Neural Networks (CNN) has enabled automatic feature learning and extraction methods for feature classification from 3D point clouds and images (Roberson et al., 2010; Douillard et al., 2011; Li et al., 2013). Although instance segmentation-based feature extraction has gained

significant importance in the field of computer vision, 3D point cloud segmentation is still under development. In the field of urban forestry, street-level imagery in combination with computer vision has been applied for the estimation of shade provision (Li & Ratti, 2019; Li et al., 2017, 2018), quantification of perceived urban canopy cover (Duarte et al., 2017; Cai et al., 2018; Li et al., 2015; Stubbing et al., 2019), and mapping the location of trees (Wegner et al., 2016). The following paragraphs summarize the research studies in tree species detection and classification, followed by limitations.

4.4.1 State-of- Art Methods for Tree Species Detection and Classification

Over the years, accurate identification and tree species classification have been essential for various research and conservation efforts. Researchers have employed different approaches, including hyperspectral data, lidar data, and machine learning algorithms, to achieve precise classifications. This paper reviews these methods and their advantages and limitations in tree species classification.

Hyperspectral data, covering visible and near-infrared spectral regions, has been used in studies by Alonzo et al. (2014), Dalponte et al. (2014), and Dian et al. (2016) to classify tree species. The results indicate high accuracy in tree species classification using hyperspectral data. Maschler et al. (2018) further automated classifying 13 tree species using this approach. However, acquiring hyperspectral data is complex, and the repeating spectral interval information for different tree species can reduce classification accuracy.

In contrast, Liu et al. (2017) argued that lidar data contributes more to accurate species classification results than hyperspectral features. Lidar data is easier to obtain and provides accurate tree height and canopy cover measurements. However, its effectiveness for

species classification depends on computing complexity, the choice of features, and classification algorithms.

Machine learning algorithms have recently been employed for tree species classification, demonstrating higher accuracy and robustness than traditional classification algorithms. Studies by Jones et al. (2010) and Dalponte et al. (2012) effectively classified tree species using RGB optical images obtained by UAVs. Dalponte et al. (2015) proposed a support vector machine (SVM) classification model for individual tree crown delineation. However, these methods require manual input of optimum threshold parameters, necessitating intense knowledge or expertise.

Deep learning algorithms have gained popularity in tree species classification because they can characterize complex patterns in imagery data. Melgani and Mancini (2020) used deep learning algorithms to classify tree species from smartphone images, achieving 89.7% accuracy. Huang et al. (2018) employed a deep convolutional neural network (CNN) to classify tree species from bark photographs, achieving 95% accuracy on a test set. Wang et al. (2020) utilized street-level images and a deep CNN to classify tree species in urban areas, achieving up to 90% accuracy on a test set. However, deep learning models may underperform on images captured in different lighting conditions or with varying contextual information, limiting their adaptability to diverse use cases.

4.4.2 Limitations of Tree Species Classification Methods

Many researchers have studied different approaches to classify tree species, using hyperspectral and photogrammetry data, leveraging machine learning (ML) and deep learning algorithms (DL). However, most studies have used low-resolution

photogrammetry data from airborne methods, resulting in limited spatial resolution that struggles to capture fine-scale features of individual trees and distinguish between different tree species due to overlapping tree canopies and similar spectral characteristics. The classification accuracies of methods leveraging airborne data range between 60% - 80%. Recently, a few studies have proposed processing high-resolution street-level image data to address these limitations in classifying tree species. Through supervised training of ML/DL algorithms, these studies have reported a 90%-95% accuracy rate in classification. However, the street-level images used for training and testing these algorithms are stand-alone trees, which lack contextual information from the surrounding environment, such as nearby trees, buildings, urban objects, and vegetation features.

This research study investigates the ability of learning algorithms to extract tree specimens and classify tree species from street-level data containing complex contextual information (Objective 3).

CHAPTER 5

DATA COLLECTION

This research study, a crucial collaboration between Arizona State University and Salt River Project (SRP), addresses critical infrastructure issues within SRP's vast canal and powerline infrastructure network. SRP's infrastructure systems feature an intricate lattice of embankments, water channels, and powerline corridors, necessitating comprehensive data collection and analysis. This research aims to employ advanced AI algorithms to process the collected data and automate data extraction and analysis procedures. Such a methodical approach is essential in managing vast information from the 262 miles of infrastructure network. The intention is to transform these data streams into actionable insights, enhancing strategic operations and maintenance activities.

In the context of canal embankments, AI algorithms aim to reduce point cloud noise, ensuring a high level of data accuracy for better operational decisions. The powerline corridors pose a unique challenge due to fast-growing tree species that could intrude with the energy supply infrastructure, necessitating their detection and identification for risk mitigation. Furthermore, the research explores the estimation of surface slope gradient and erosion measurement from fast-degrading earthen embankments to assess their structural integrity, enabling early intervention and preventing potential failures. This collaborative research signifies an innovative step forward in infrastructure management, utilizing AI's power to address complex problems, automating processes, and enhancing the strategic operations and maintenance activities for SRP's critical infrastructure systems. The following sections detail the data collection procedure adopted for this research study, i.e.,

defining a region of interest, making ground reference points, data collection, and post-processing.

5.1 Region of Interest (ROI)

The area of focus for this study spans 262 miles of canal embankments within the Phoenix metropolitan region under the jurisdiction of SRP. The data for the study has been gathered from several canals, including the Arizona Canal, Grand Canal, South Canal, Tempe Canal, Western Canal, Eastern Canal, and Consolidated Canal. These canals traverse several cities, such as Chandler, Gilbert, Mesa, Tempe, Scottsdale, Phoenix, Glendale, Tolleson, and Peoria. Refer to Figure 3.

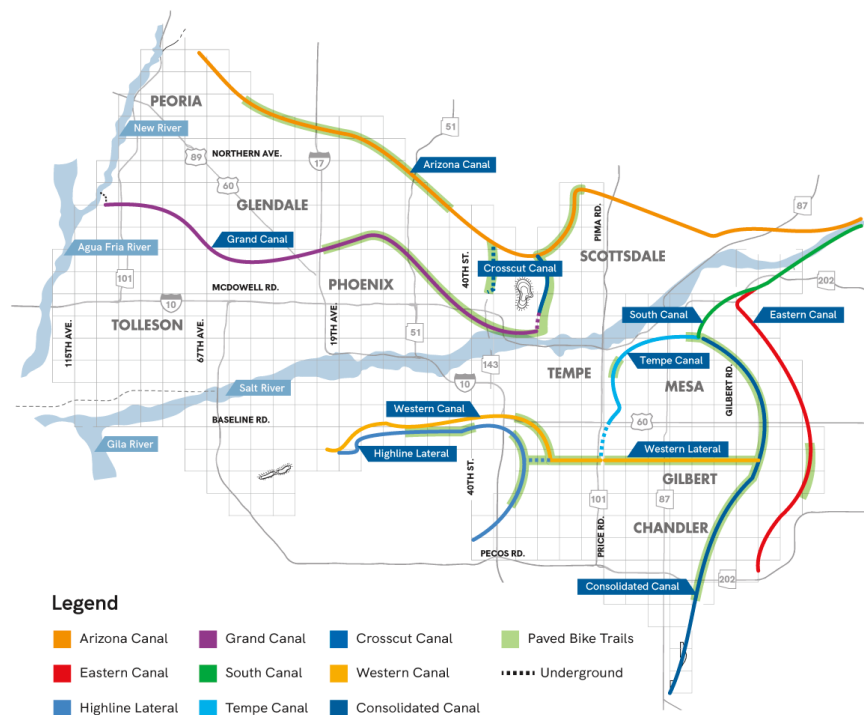


Figure 3. Region of Interest Canals Under Jurisdiction of SRP

5.2 Geo-reference Points

Before gathering data, the SRP team ensured that ground reference points were established for each mile of the embankment. This was done to enhance the precision of the data collection process. The data was gathered for 131 miles along the canal's centerline, equating to 262 miles of canal embankments. Hence, the SRP team identified and marked approximately 262 ground reference points.

5.3. Data Acquisition

This study uses high-resolution 3D point cloud data collected through the canal embankment with above-the-ground photogrammetric and laser scanner Topcon IP-S2 mounted in a roving truck unit. The Topcon navigation technology combines three distinct technologies, i.e., dual-frequency 40-channel GNSS (Global Navigation Satellite System) receiver, Honeywell HG 1700 tactical-grade ring laser gyroscope, and DMI (Distance measuring interval module) (Punete et al., 2013). The GNSS receiver updates the position of the scanner relative to vehicle altitude provided by laser gyro, further supplemented by DMI for overall positioning. The image capability is based on the LADYBUG3 multicamera unit, which performs 3,600 panoramic imaging up to 15 frames per second (Punete et al., 2013), with an average speed of 30 miles/hour. Figure 4. Illustrate a similar truck-mounted Lidar unit leveraged for data collection.

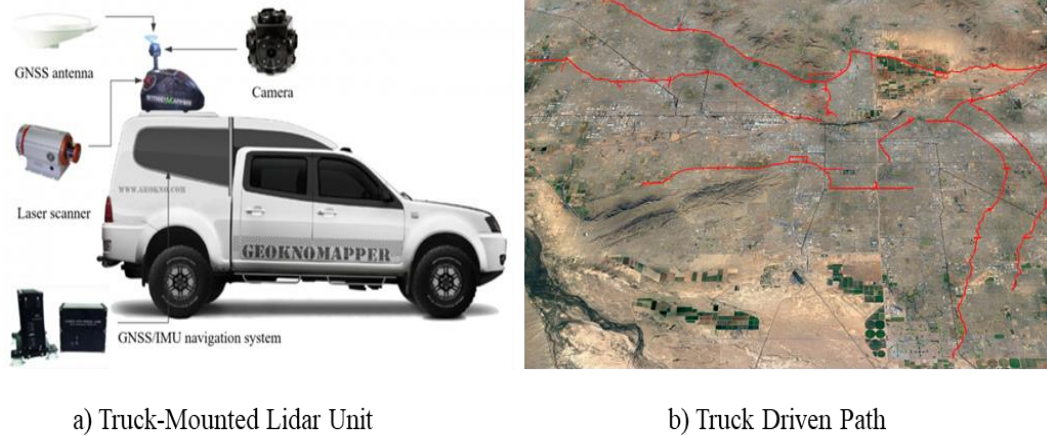


Figure 4. Mobile Lidar Unit

The entire laser scanning is carried out by three SICK Laser Measurement Sensors (LMS) 291 scanners (Punete et al., 2013). One laser was pointing towards the road, and the other two lasers were pointing at each side to provide a series of range and elevation profiles. The weather conditions were ideal; the data gathered was in the broad sunlight between 10 am – 3 pm. This process has taken twelve days to gather data for entire canal miles. The average point cloud density generated by the Lidar unit was 1,200 -1,500 points/square meter.

5.4 Post-processing

The responsibility for field data collection, registration, and post-processing, was handled by BPG Design. The gathered data was subsequently post-processed in alignment with the pre-marked ground reference points. This approach facilitated a high level of surveying accuracy (approximately 1mm) in determining the coordinates of each point within the cloud. Figure 5. illustrates a photogrammetric image of the point clouds for a canal cross-section.



Figure 5. Photographic Image of 3D Point Cloud

CHAPTER 6

AUTOMATED NOISE FILTERING FROM HIGH REFLECTIVE ENVIRONMENTS

This research study's significance lies in advancing data collection and processing methodologies, specifically from challenging environments like unpaved embankment roads surrounded by high-reflective water surfaces. Such environmental settings often generate significant noise during data collection, interfering with the dataset's accuracy and usefulness. To harness this dataset for constructive analysis and predictive modeling, the study focuses on developing AI algorithms that effectively filter out this noise. By addressing the data quality issues and enhancing data processing techniques, this research helps pave the way for more accurate assessments of infrastructure conditions to support strategic O&M.

High-reflective environments, such as those with water bodies or metallic structures, can lead to incorrect data points due to the high reflectivity of surfaces. These noise points pose significant challenges in modeling and visualization tasks. Therefore, an efficient filtering approach is essential to ensure the quality and reliability of point cloud data.

The noise in point cloud data usually falls into two main categories: outliers and systematic noise (Zhang et al., 2016). Outliers are isolated points that significantly deviate from the neighboring points. These can occur due to sensor errors or reflection from small, non-static objects like leaves or birds. On the other hand, systematic noise appears as consistent patterns or structures in the data, often resulting from sensor bias, misalignment, or

multiple reflections in highly reflective environments. Figure 6. illustrates noise in the point cloud datasets.



Figure 6. Noise in Raw Point Cloud Dataset

The current research methods for noise filtering primarily revolve around statistical outlier removal, radius-based outlier removal, and machine learning-based approaches. Statistical outlier removal is a straightforward and common technique that removes data points too far away from the mean of their neighboring points. Radius-based outlier removal eliminates points with fewer than a certain number of neighbors within a specified radius, thereby helping filter sparse noise points.

However, these techniques have their limitations. For instance, statistical and radius-based outlier removal methods may inadvertently remove valid data points, particularly in sparse or complex environments. Furthermore, the issue of filtering noise in high-reflective environments, like water bodies or metal surfaces, is even more challenging. Traditional filtering methods often need help with these environments due to the complex nature of multiple reflections and their impact on the data points.

Machine learning-based approaches offer more advanced solutions to noise filtering. Deep learning models, for instance, can be trained to recognize and eliminate noise patterns based on large datasets. This research study explores the supervised reinforcement learning analytical algorithms for noise filtering that can effectively distinguish noise generated from complex real-world environments.

The following paragraphs discuss the methodology for noise filtering, complemented by pseudo code for clarity. The noise filtering results are validated with ground truth information and compared with the outcomes from traditional algorithms. This comprehensive comparison helps understand the merits of the proposed method, identifies limitations, and discusses opportunities for further enhancement in point cloud processing techniques.

6.1 Noise Filtering Algorithm Framework

The methodology component of this study separates into four distinct sections. First, the study executes pre-processing and initial segmentation, laying a robust foundation for subsequent steps. Following this, unsupervised DBSCAN (Density-Based Spatial Clustering Application) filtering removes free-floating noise clusters. The third step involves eliminating reflection noise and tackling the common issues associated with high-reflective environments. Figure 7. shows types of noise in the dataset. Finally, the study applies a supervised trained ReLU network to filter surface noise, further refining the quality of the point cloud data. Figure 8. Show the noise filtering algorithm framework used in this study.

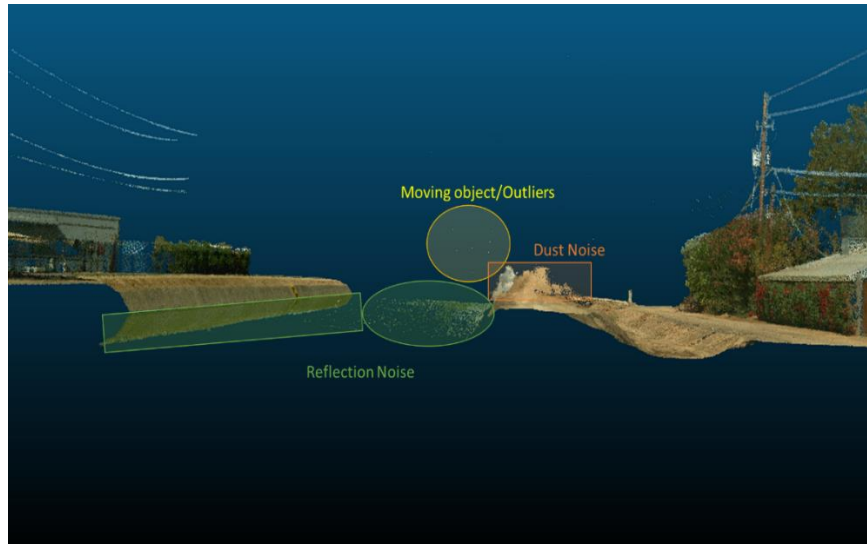


Figure 7. Types of Noise in Raw Point Cloud Dataset

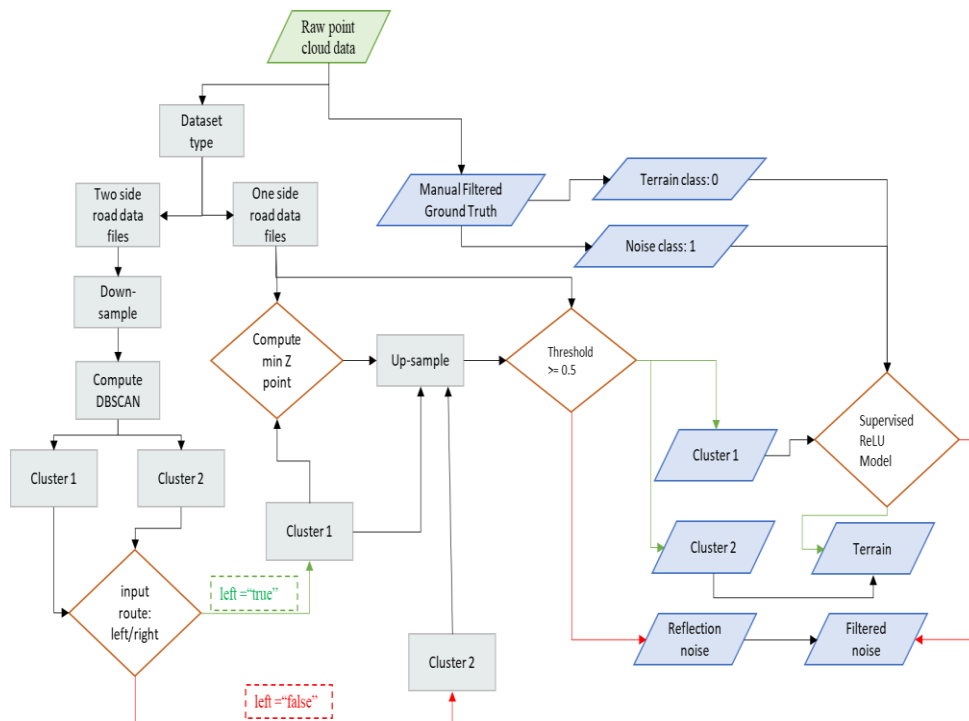


Figure 8. Noise Filtering Algorithm Framework

6.1.1 Pre-processing (Segmentation)

As the research study especially focused on terrain-based noise filtering, all the unwanted object features outside the terrain boundary are pre-processed for segmentation. These unwanted object features, such as wires, poles, vegetation, walls, and other electrical equipment, could introduce noise and inconsistencies in the data. By eliminating these features in the initial stage, the study ensures that the dataset under investigation is more focused and pertinent to the noise filtering from terrain surface, laying the groundwork for more accurate and reliable subsequent processing and filtering stages.

6.1.2 Dataset Type

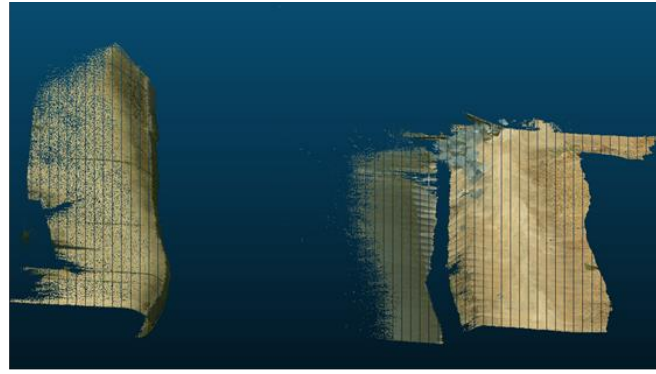
The study incorporates a dynamic model training and testing approach to ensure algorithm adaptability across multiple use-case scenarios. Two distinct types of datasets serve as the foundation for this process.

The first dataset, 'Type 1,' comprises one-side terrain data files. These files correspond to situations where the terrain is only present on the data collection side. Such scenarios typically involve reflection noise due to highly reflective surfaces and surface noise from dust and moving particles. It is important to note that as Type 1 files are one-sided, the DBSCAN clustering stage is bypassed for these files.

The second dataset, known as 'Type 2,' encompasses two-side terrain data files. These files portray the terrain surface on both sides of the embankment. This configuration introduces unique challenges, with reflection noise on both sides and surface noise on the data collection side. Figure 9. Show the types of datasets used in this research study.



a) Type 1 : one –side terrain data



a) Type 2 : Two –side terrain data

Figure 9. Type of Datasets for Analytics

This study enables a comprehensive understanding and improvement of the model's noise filtering capabilities by incorporating both datasets into the model's training and testing phases. This method ensures that the model is adequately prepared to handle diverse noise-filtering scenarios, thus enhancing its practicality and precision.

6.1.3 DBSCAN Clustering

This study employs the DBSCAN clustering approach to distinctly categorize the two-side terrain surface files into clusters of individual terrain files. The DBSCAN algorithm works on the principle of density-based clustering, which considers clusters as high-density regions separated by areas of lower density. Its mathematical formulation typically uses two parameters: epsilon (ϵ), which defines the maximum distance between two samples for them to be clustered in the same neighborhood, and “minPts,” the minimum number of points required to form a dense region.

The mathematical basis of DBSCAN involves determining whether the ϵ -neighborhood of a point has enough points (at least minPts) to consider it a core point. The algorithm proceeds by arbitrarily selecting a point in the dataset. A new cluster is created if there are

at least minPts within a radius of ϵ from that point. The cluster then expands by adding all direct density-reachable objects to the cluster. If a point is density-reachable from any point of the cluster, it is added, too. This process continues until no more points can be added to the cluster. The algorithm then proceeds with the next point in the dataset and repeats the process until all points have been processed. Table 1. illustrates the pseudo-code of the DBSCAN algorithm. Figure 10. show the clustering from the DBSCAN algorithm visualized in the cloud compare point cloud processing tool.

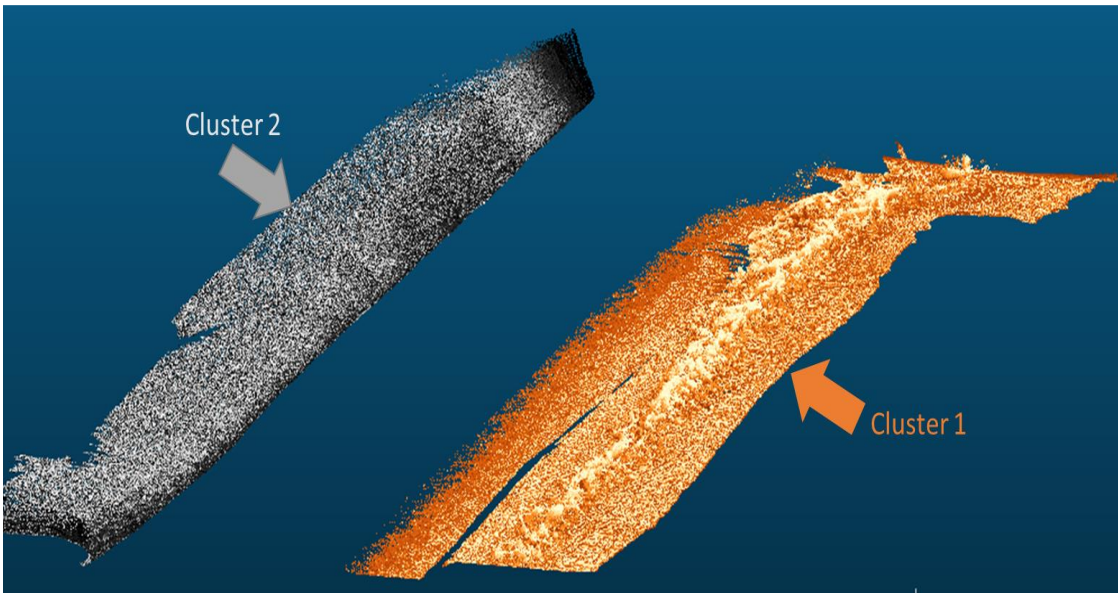


Figure 10. DBSCAN Clustering of Point Cloud Dataset

Table 1. Pseudo Code for DBSCAN Clustering Algorithm

Algorithm 1: ALGORITHM FOR DBSCAN CLUSTERING			
	Input: D (dataset as a set of points), ϵ (distance for neighborhood), $minPts$ (minimum number of points required to form a dense region)		
	Output: C (set of clusters)		
	Initialize $C =$ empty set		
	For each unvisited point P in dataset D		
		- Mark P as visited	
		- Get $NeighborPts$, the ϵ -neighborhood of P	
		- If the size of $NeighborPts$ is greater than or equal to $minPts$	
		- Create a new cluster, $newCluster$	
		- Extend $newCluster$ with P and all points in $NeighborPts$	
		- For each point P' in $NeighborPts$	
			- If P' is not visited
			- Mark P' as visited
			- Get $NeighborPts'$, the ϵ -neighborhood of P'
			- If size of $NeighborPts'$ is greater than or equal to $minPts$
			- Append $NeighborPts'$ to $NeighborPts$
			- If P' is not yet a member of any cluster
			- Add P' to $newCluster$
		- Add $newCluster$ to the set of clusters C	
	Return C		

6.1.4 Filtering Reflection Noise

Applying DBSCAN clustering to two-sided terrain data in this research results in data split into two clusters, typically separated by a physical distance. Each generated cluster corresponds to an individual terrain file. After the successful application of DBSCAN clustering, the next phase involves identifying the 'min point' within the dataset.

The 'min point,' in this study's context, signifies the reflection point on the water's surface. Due to water surfaces' flat, mirror-like nature, this point often displays the lowest elevation point in the dataset. Identifying this 'min point' is critical in managing the reflection noise frequently associated with high-reflective environments, thereby enhancing the point cloud data's accuracy.

The employed algorithm operates under the assumption that the 'min point' in the Z-axis, or the lowest elevation, always signifies a reflection point within the dataset. Consequently, a threshold value of 0.5 feet is established. Points falling within a range of 0.5 feet below the 'min point' are classified as reflection noise. In contrast, points exceeding the 0.5 feet threshold are considered terrain points for the time being and proceed further for surface noise filtering. Figure 11. Shows the reflection noise filtered from cluster 1 and clustered 2 using the min Z-axis point from the dataset.

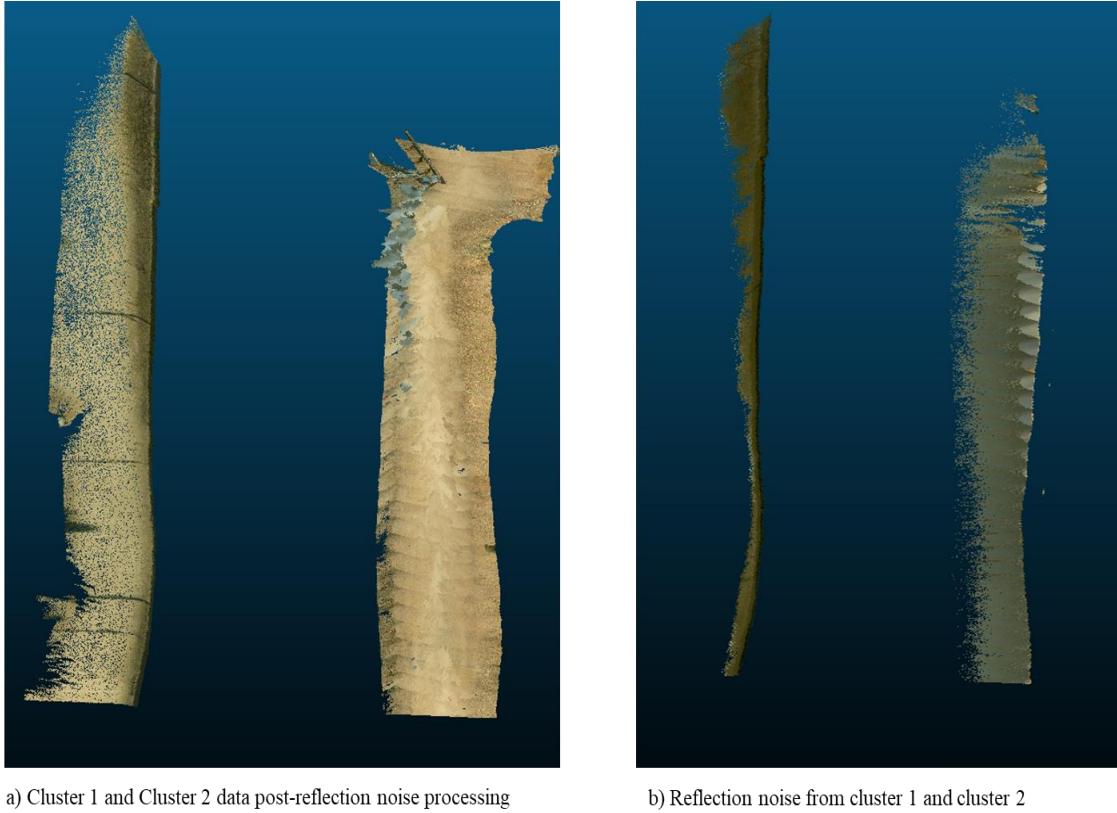


Figure 11. Data Clusters Post-Reflection Noise Processing

6.1.5 Supervised Neural Network Model for Surface Noise Filtering

This research explores the efficiency of neural network algorithms to separate noise from surface point clouds. The research study leverages the supervised learning capability of neural networks to follow a systematic process to accomplish the noise-filtering task.

Firstly, ten ground truth datasets are labeled, distinguishing between noise and surface points. The labels assigned are 0 for noise and 1 for surface points. The ten ground truth datasets are selected based on the variable noise characteristics in the dataset. These labeled datasets serve as the basis for training the neural network model.

The algorithm proceeds by training the model using these labeled datasets for a specified number of epochs, which in this case is 150. During training, the model learns to recognize patterns and features that differentiate noise from surface points within the point clouds.

The dataset is split into training and testing subsets, i.e., eight training and two testing datasets. The model is tested on the testing subset to assess its ability to classify accurately and separate noise from surface points. The model is saved for future use upon completion of the training phase. It is then applied to various point cloud datasets to test its generalization capability and effectiveness in separating noise from surface points.

The trained model identifies each data point within the testing dataset as either a terrain point, denoted with class value "1", or a noise point, marked with class value "0". The algorithm's accuracy of the terrain classification is assessed by comparing its identification of terrain points against the established ground truth information, yielding the quantity of true positive terrain values. In parallel, the algorithm's ability to correctly distinguish noise points is also measured, providing the number of true positive noise values, which is again compared to the manually segmented ground truth data. The accuracy of the model's predictions is subsequently determined by analyzing the percentage of points accurately identified in both terrain and noise classifications, providing a well-rounded assessment of the model's efficiency and precision. Figure 12. illustrate the filtered noise from the original point cloud dataset. The results obtained from these experiments are presented in subsequent sections of the research paper, providing insights into the algorithm's performance, its ability to distinguish noise from surface points, and its efficiency

compared to the traditional model. Table 2. provides the pseudo-code of the supervised clustering algorithm.



Figure 12. Processed Point Clouds Post-Noise Filter

Table 2. Pseudo Code for Supervised Neural Network for Noise Filtering

ALGORITHM 2: SUPERVISED NEURAL NETWORK ALGORITHM FOR NOISE FILTERING	
<i>IMPORT TensorFlow library</i>	
<i>Define function -create a model.</i>	
	<i>Create a neural network model.</i>
	- <i>Dense layer with 64 units, ReLU activation, and input shape (input_dim)</i>
	- <i>Dense layer with 64 units and ReLU activation</i>
	- <i>Dense layer with two units and softmax activation</i>
	<i>Return the model</i>
	- <i>Set GPU memory growth to True for the first physical device</i>
	- <i>Set input_dim to 3</i>
	- <i>Set batch_size to 64</i>
	- <i>Set epochs to 150</i>
	<i>Create the noise_filter_model using create_model function</i>
	<i>Compile the model with:</i>
	- <i>Optimizer: Adam</i>
	- <i>Loss function: Sparse categorical cross-entropy</i>
	- <i>Metrics: Accuracy</i>
	<i>Define x_train as the training data</i>
	<i>Define y_train as the training labels</i>
	<i>Create a TensorFlow Dataset from x_train and y_train with batch_size</i>

	<i>Train the model on the train_dataset for the specified number of epochs</i>
	<i>Save the trained model as 'point_classification_model.h5'</i>
	<i>#test</i>
	<i>Define x_test as the test data</i>
	<i>Define y_test as the test labels</i>
	<i>Evaluate the trained model on x_test and y_test:</i>
	<i>Calculate the predicted labels using the trained model on x_test</i>
	<i>Calculate the accuracy of the predictions by comparing them with y_test</i>
	<i>Display the accuracy</i>

The trained model achieved an accuracy of 98.4% in filtering noise from the testing dataset. The loss curve for each epoch is presented below. Figure 13. The loss curve illustrates the decrease in the model's loss function over the training process.

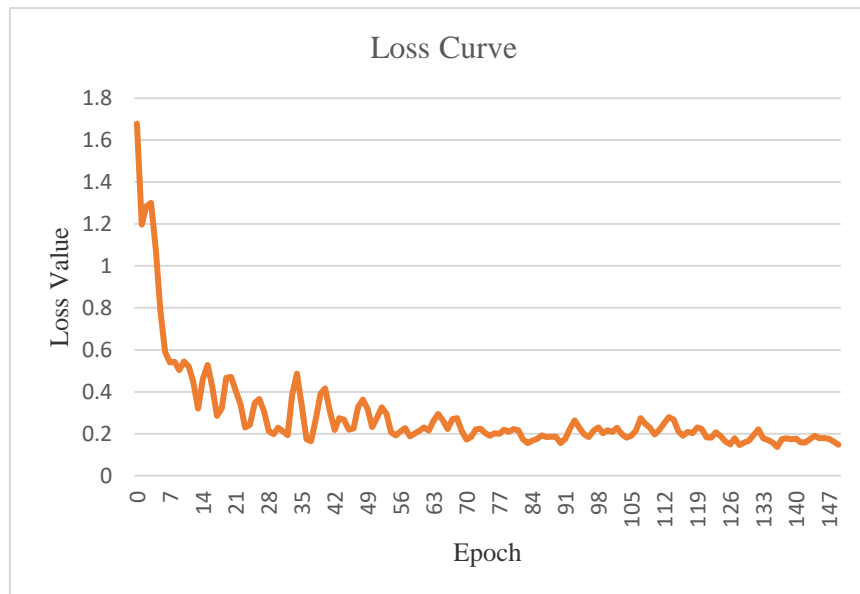


Figure 13. Training Loss Curve of Noise Filtering Neural Network Model

The model learns to make better predictions as the epochs progress, resulting in a lower loss value. The model's accuracy at the final epoch reflects its ability to correctly classify the data, with 98.4% accuracy indicating high noise filtering performance. The following sections discuss the results and validation of the neural network model against the traditional noise filtering algorithms.

6.2. Validation

The proposed neural network method was validated using four comparison methods: 1) cloth simulation function, 2) slope-based method, 3) Statistical Outlier Removal (SOR), and 4) Open 3D spatial filter method. These algorithms served as benchmarks for evaluating the performance of the model. The proposed method was validated by comparing two parameters: 1) type 1 evaluation, which represents the number of terrain points classified as terrain points, and 2) type 2 evaluation, which represents the number of noise points identified as noise points. In the comprehensive evaluation process, the trained models predict each data point within the testing dataset as either a terrain point ("1") or a noise point ("0"). The proficiency of the algorithm in terrain identification is pursued by comparing its classified terrain points against the ground truth, yielding the count of true positive terrain values. Concurrently, the ability of the model to accurately classify noise points is assessed, producing the number of true positive noise values, which is contrasted with the ground truth data for accuracy assessment. Table 3. shows the comparative methods and testing environments. All the classified results are finally visualized Cloud Compare Lidar processing tool.

Table 3. Noise Filtering Methods and Testing Environments

Method	Testing Environment	Visualization
Supervised Neural Nets (ours)	Python, Tensor Flow	Cloud Compare
Cloth Simulation Filter (CSF)	Cloud Compare	Cloud Compare
Slope-based Method	Python	Cloud Compare
Statistical Outlier Removal (SOR)	Python	Cloud Compare
Open 3D Spatial Filtering	Python, Scikit-Image	Cloud Compare

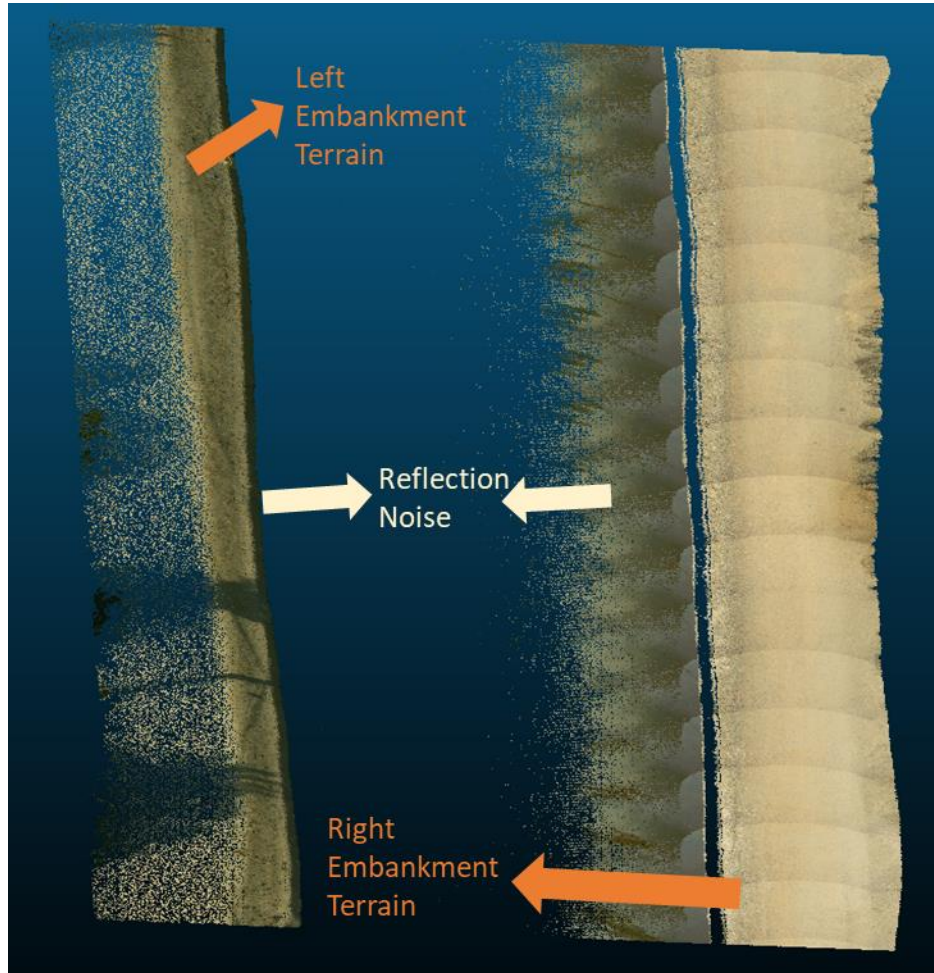
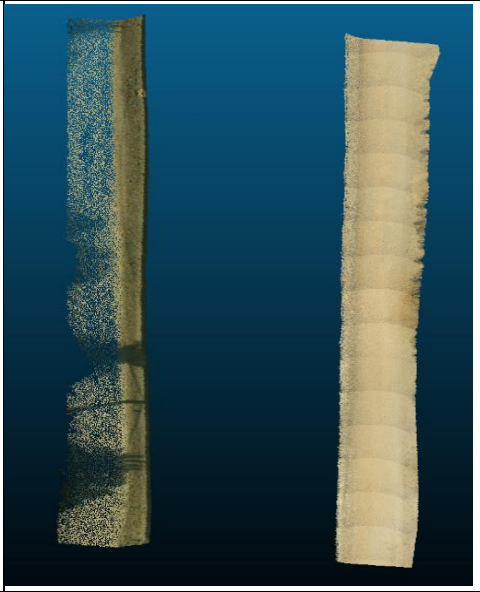
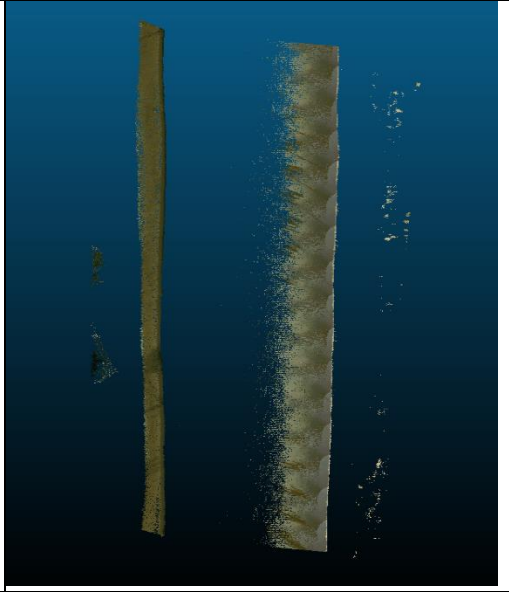
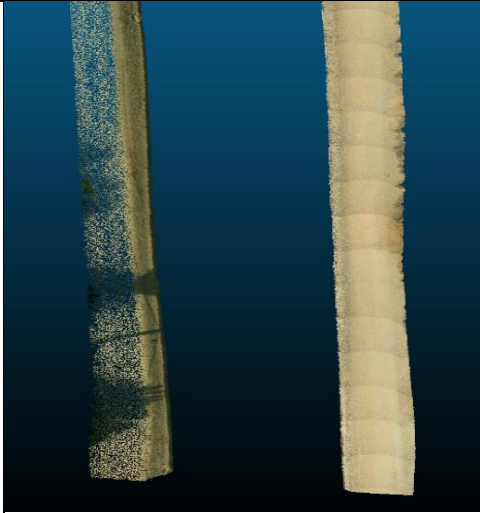
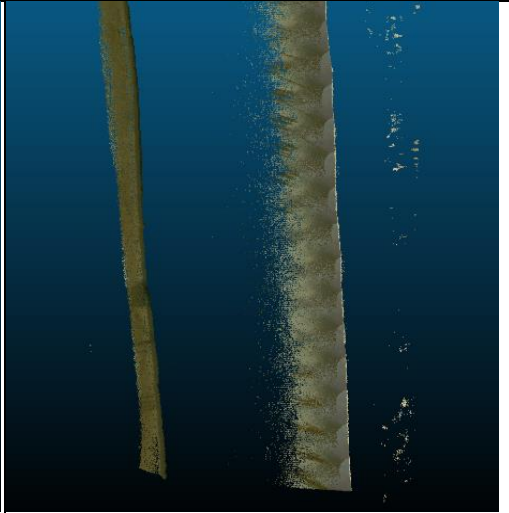


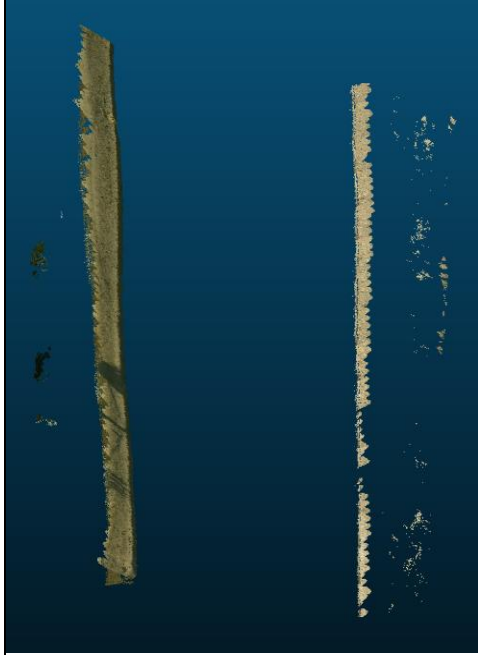
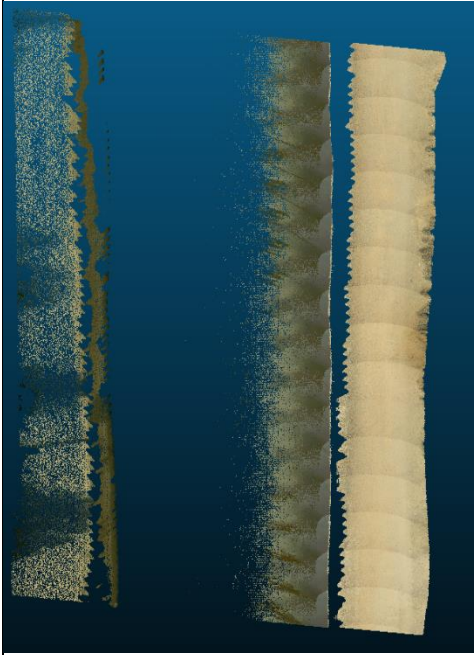
Figure 14. New Test Dataset

The following images in Table 4. showcase the filtering results of noise algorithms for raw point cloud data (Figure 14) visualized in the Cloud Compare software tool. The dataset comprises point clouds with two terrain surfaces.

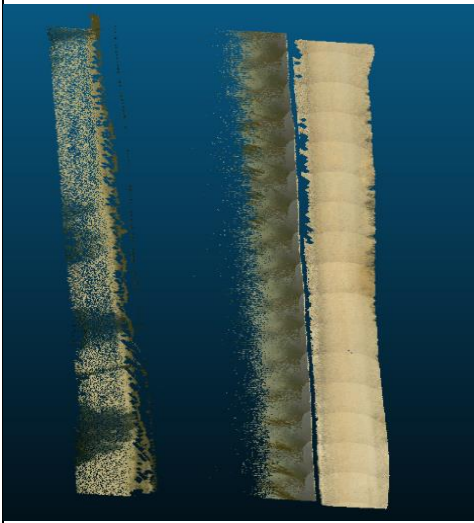
Table 4. Results from Processing Two side Terrain Raw Point Cloud Dataset

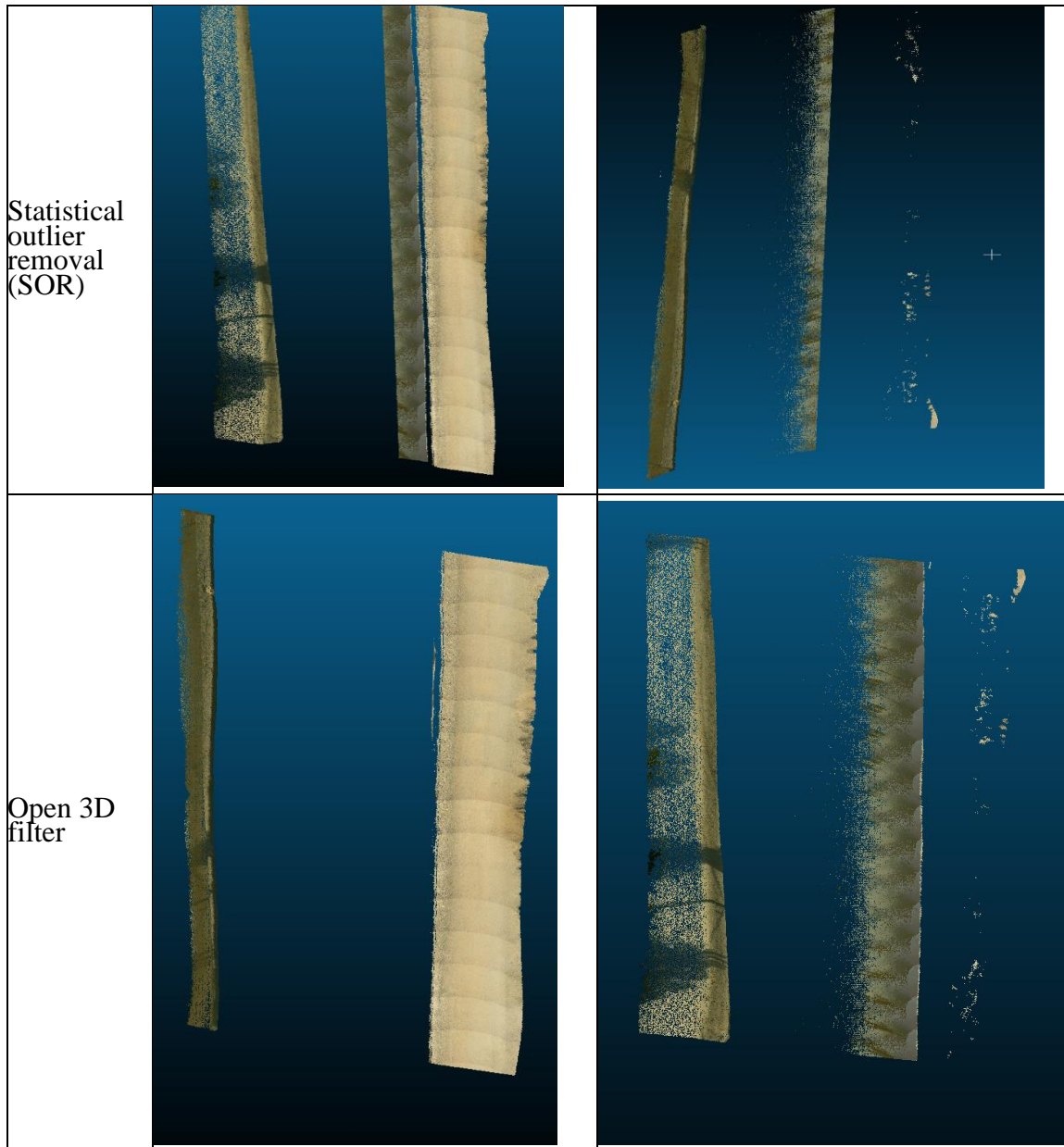
Noise Filtering Method	Classified Terrain	Filtered Noise
Ground Truth		
Supervised Neural Nets (ours)		

Cloth
Simulation
Filter (CSF)



Slope-
based
Method





The evaluation revealed that the other algorithms employed in the study could not effectively identify vertical slopes as terrain and often misclassified reflection noise. The algorithms are tested on sample datasets of the Type 1:one side terrain dataset for better comparison. The evaluation of three sample raw point cloud datasets is discussed in the following sections.

6.2.1 Sample 1: Low Surface Noise Dataset

The analysis is carried out on a sample dataset with paved concrete terrain; because of low surface noise, most algorithms have done a good job classifying terrain points; however, they failed to separate reflection noise from the terrain dataset. See Figure 15. Our neural net algorithm has achieved 99.3% accuracy in classifying terrain points and 97.40% accuracy in filtering noise from the dataset. Table 5. shows the comparative evaluation of results for the sample 1 dataset.

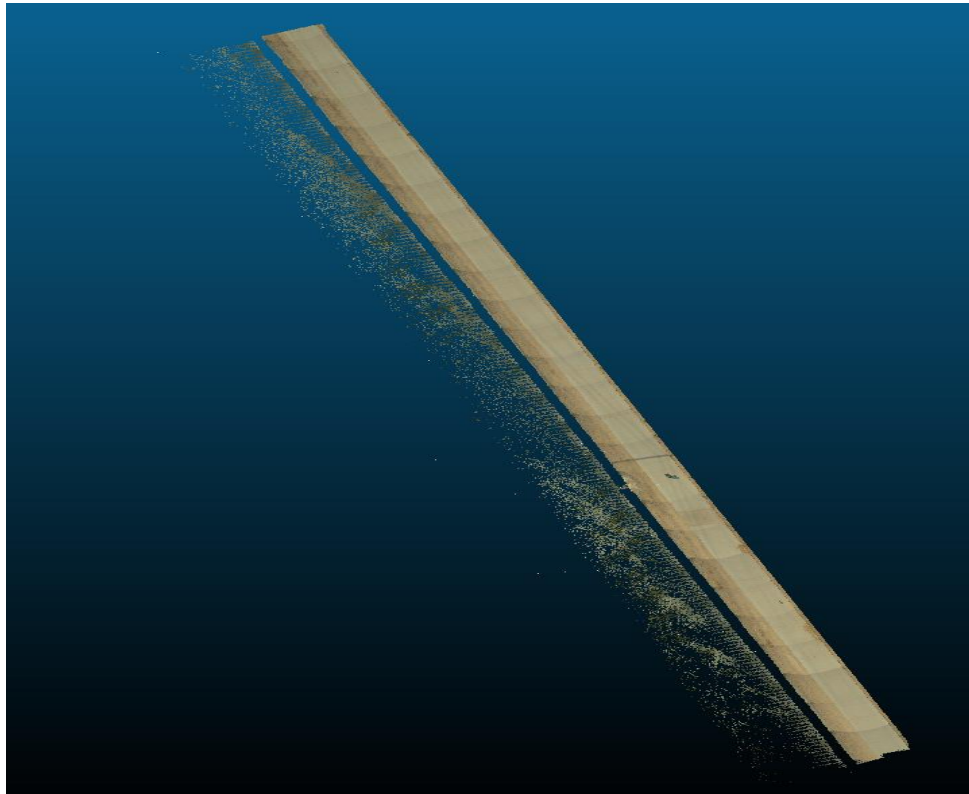


Figure 15. Low Surface Noise Dataset

Table 5. Evaluation of Noise Filtering Algorithms on Low Noise Dataset

Algorithm	Terrain Data Points	Noise Points	Accuracy (Terrain Points)	Accuracy (Noise)
Ground Truth	2,796,616	36,800		
CSF Filter	2,791,023	8,538	99.80%	23.20%
Slope based Method	2,441,446	30,176	87.30%	82%
Statistical Outlier Removal (SOR)	2,612,039	8,206	93.40%	22.30%
Open 3D Morphological Filter	2,662,378	8,832	95.20%	24%
Supervised Neural Net (ours)	2,777,040	35,843	99.30%	97.40%

6.2.2 Sample 2: Medium Surface Noise Dataset

The analysis is carried out on a sample dataset with unpaved terrain; due to the thick reflection noise surface on the water, most algorithms have failed to separate reflection noise from the terrain dataset. See Figure 16. Our neural net algorithm has achieved 98.7% accuracy in classifying terrain points and 98.30% accuracy in filtering noise from the dataset. Table 6. shows the comparative evaluation of results for the sample 2 dataset.

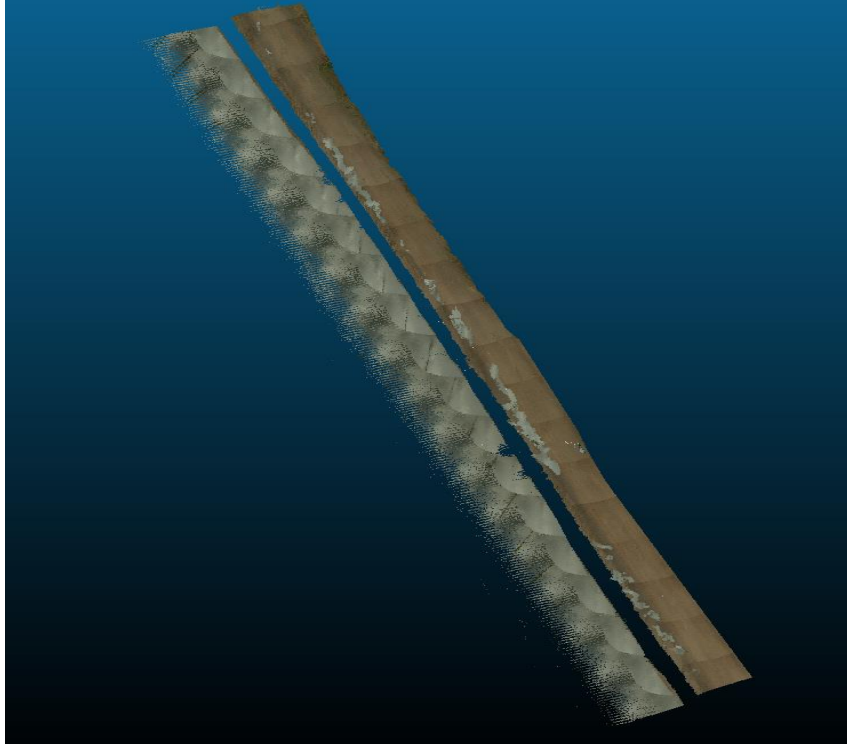


Figure 16. Medium Surface Noise Dataset

Table 6. Evaluation of Noise Filtering Algorithms on Medium Noise Dataset

ALGORITHM	Terrain Data Points	Noise Points	Accuracy (Terrain Points)	Accuracy (Noise)
Ground Truth	2,692,746	633,223		
CSF Filter	2,369,616	214,329	88.00%	33.84%
Slope based Method	2,396,544	512,911	89.00%	81%
Statistical Outlier Removal (SOR)	2,208,052	260,888	82.00%	41.20%
Open 3D Morphological Filter	2,504,254	558,503	93.00%	88%
Supervised Neural Net (ours)	2,563,494	622,458	98.70%	98.30%

6.2.3 Sample 3: Heavy Surface Noise Dataset

The analysis is carried out on a sample dataset with unpaved terrain with heavy noise; due to the clear difference in elevation between reflection noise and terrain points, most algorithms did a better job filtering noise points than the last two samples. See Figure 17. Our neural net algorithm has achieved 96.3% accuracy in classifying terrain points and 95.10% accuracy in filtering noise from the dataset. Table 7. shows the comparative evaluation of results for the sample 3 dataset.

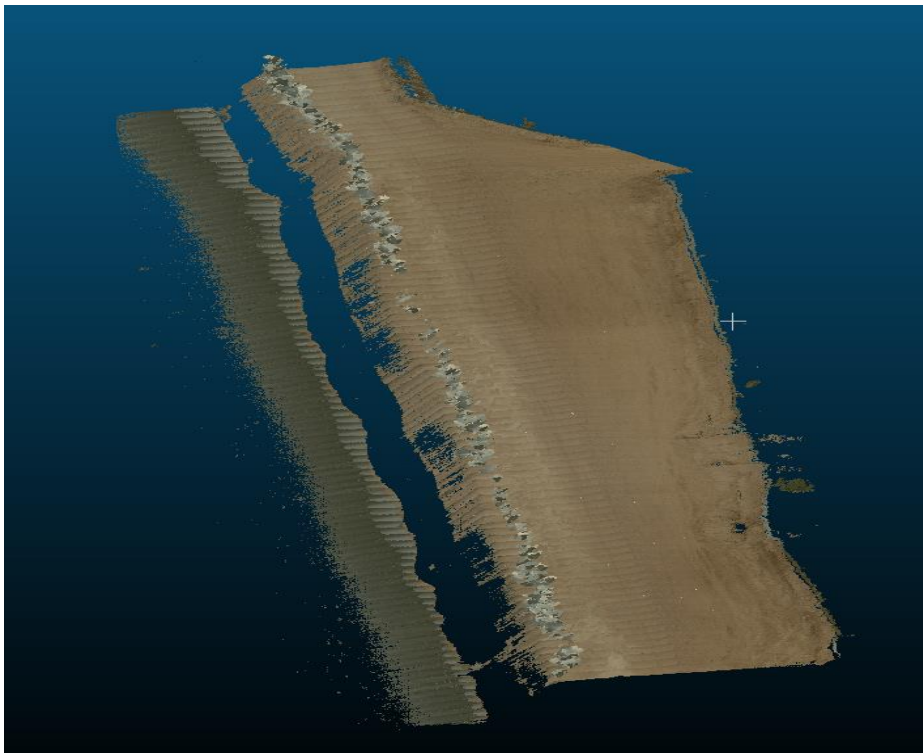


Figure 17. Heavy Noise Dataset

Table 7. Evaluation of Noise Filtering Algorithms on Heavy Noise Dataset

ALGORITHM	Terrain Data Points	Noise Points	Accuracy (Terrain Points)	Accuracy (Noise)
Ground Truth	22,209,639	1,522,321		
CSF Filter	20,743,803	770,294	93.40%	50.60%
Slope based Method	18,478,420	1,339,642	83.20%	88%
Statistical Outlier Removal (SOR)	19,833,208	977,330	89.30%	64.20%
Open 3D Morphological Filter	21,143,576	1,050,401	95.20%	69%
Supervised Neural Net (ours)	21,387,882	1,432,504	96.30%	95.10%

Based on the results obtained, our proposed neural network algorithm demonstrates significant improvements in classifying terrain points and effectively filtering noise from the dataset compared to other algorithms. The achieved accuracy of classifying terrain points and filtering noise showcases the algorithm's robustness and efficiency. These findings highlight the potential of neural network-based approaches in accurately analyzing point cloud data with complex noise characteristics, such as reflection and surface noise due to dust. The successful implementation of our algorithm contributes to the advancement of noise filtering techniques, enhancing the reliability and quality of point cloud analysis in various applications, including terrain analytics and monitoring. However, Despite the promising results achieved in this study, there are certain limitations discussed in the following section.

6.3 Limitations

- **Dataset Generalization:** The analysis was carried out on a specific sample dataset with reflective surfaces from surrounding water bodies. Generalizing the findings to different terrains or diverse environmental conditions may require further validation and testing.
- **Algorithm Performance on Other Noise Types:** Although our neural network algorithm demonstrated excellent performance in filtering reflection noise and moving dust, its effectiveness in handling other types of noise, such as sensor noise or occlusion noise, remains to be investigated.
- **Model Training and Hyperparameters:** The performance of the neural network algorithm heavily relies on the quality of training data and the selection of appropriate hyperparameters. The impact of different training data sizes, variations in hyperparameter tuning, or alternative model architectures should be explored to comprehensively understand the algorithm's limitations.
- **Computational Resource Requirements:** The neural network algorithm used in this study might demand significant computational resources, particularly for large-scale point cloud datasets. The feasibility and scalability of the algorithm on resource-constrained devices or real-time applications need to be assessed.

CHAPTER 7

TERRAIN ANALYTICS

Large road infrastructure networks extended over vast areas include asphalt, concrete, or earthen soil surface roads. Uncontrolled water discharges due to rains allow standing water to penetrate the road surface; through potholes or retention in puddles, the road surface and the road base become weak. Which further causes damage and material loss, making infrastructure susceptible to erosion. Additionally, abrasion, compaction, and displacement of surface material caused by moving traffic and improper grading can also deform the road surface. The types of road surface crowns are discussed below. See Figure 18.

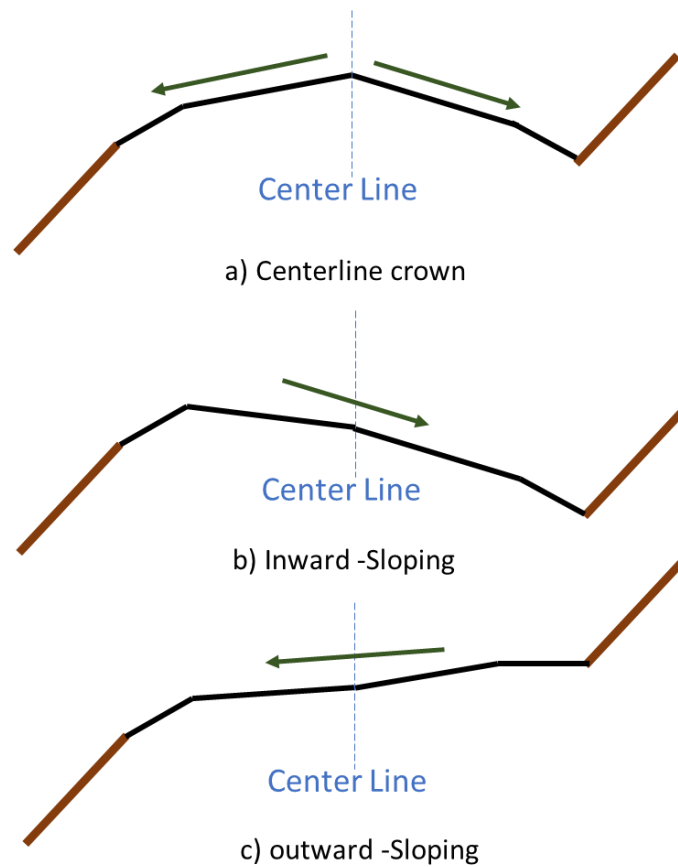


Figure 18. Types of Road Crown Surface

- Centerline Crown

A surface shape allows surface water to flow in either direction from the high point at the center.

- In-ward slope

A road surface shape allows surface water to flow from the entire width of the road toward the cut-bank or up-slope side. The in-ward slope condition is considered a (+) slope for research purposes.

- Out-ward slope

A road surface shape allows surface water to flow from the entire road width toward the fill bank or cut-slope side. The outward slope condition is considered a (-) slope for research purposes.

The Salt River Project (SRP) manages numerous unpaved embankments within its canal network. These earthen embankments, though robust, can be prone to terrain slope changes due to inclement weather, particularly heavy rainfalls. Rain-induced erosion can lead to the formation of inverted slope patterns. These changes affect the structural stability of the embankments and result in unwanted sediment discharges into the canal system. Such sediment discharges are problematic as they can significantly impact water quality within the canals and disrupt regular operations. Moreover, these discharges violate the Environmental Protection Agency (EPA) regulations, emphasizing the necessity for continuous monitoring and effective maintenance of these embankments to prevent such occurrences.

Over time, traffic and nature can wash out the surface aggregates resulting in the displacement of the crown, so grading and maintenance of the road should be a routine process. Every road surface can be different; some require more frequent maintenance than others. For example, unpaved roads require 2 or 3 times more maintenance than paved roads, as paved roads resist water infiltration, unlike gravel or dirt roads. As civil infrastructures are large and have a complex-surface orientation, this study proposes a Slope Orientation-based Terrain Modeling (SOTM) algorithm that generates a dynamic surface grade profile. The SOTM algorithm supports the decision systems for erosion estimation, surface elevation grading, and determining maintenance requirements for infrastructure. The surface grade heatmaps from the SOTM algorithm offer a dynamic and detailed perspective on the topography. When integrated with real-time camera images, these heatmaps facilitate a powerful visual tool for observing and understanding terrain changes as they occur. This combination of technologies boosts the clarity and precision of terrain assessments. It revolutionizes monitoring and reacting to real-time landscape variations, providing crucial information in urban planning, disaster management, and autonomous vehicle navigation.

7.1 Algorithm Framework for Terrain Analytics

The proposed algorithm framework actively integrates lidar data with camera images, refines the selection of the processing window, and leverages Shepard's Inverse Distance Weighting (IDW) interpolation within a SOTM algorithm. This four-stage computational procedure is an advanced model for image analysis and result interpretation.

The first step in this algorithm is the fusion of lidar data with camera images, which unifies 3D point cloud data with 2D visual information, generating a composite output that captures detailed, multidimensional scene interpretation.

Following this, the second stage involves the selection of a processing window. The algorithm systematically determines an optimal subset of data for processing, maximizing computational efficiency and focusing on regions of interest.

In the third stage, the SOTM algorithm, employing IDW interpolation, performs the computation process to generate a heat map of the terrain surface. This technique influences nearby data points based on distance, lending more weight to closer points and enhancing the model's sensitivity to local patterns.

The final step of the algorithm framework involves the visualization of the integrated results, presenting a comprehensive, graphical representation of the data. Enables users intuitively understand the resultant information, aiding in analysis and decision-making.

Georeferencing camera images by fusing them with LiDAR data involves a process that assigns geographic coordinates to the camera images, using LiDAR data as the reference system. This process is crucial in ensuring that each pixel in the image accurately corresponds to a specific geographical location on Earth, enabling precise overlaying of data from various sources for comprehensive terrain analysis.

7.1.1 LiDAR and Camera Image Data Fusion

LiDAR data, with its inherent geographic information, serves as a perfect baseline for georeferencing. The high-resolution 3D point cloud data captured by LiDAR contains each point's precise location information (longitude, latitude, and altitude). By leveraging

sophisticated alignment algorithms, the coordinates from the LiDAR data can be transferred to corresponding pixel points in the camera images.

The process begins with identifying common features or points in the LiDAR data and the camera images. These could be distinct terrain features, edges of buildings, road markings, or any other elements that are clearly identifiable in both datasets. A transformation matrix is computed using these common points, which relate the image coordinates to the LiDAR coordinates.



Figure 19. Camera and LiDAR Data Fusion

Once this matrix is computed, it aligns geometric XYZ coordinates to every pixel in the camera image, effectively georeferencing it. See Figures 19 &20. The result is a set of camera images that are tied to a specific geographic location, allowing them to be accurately overlaid on other georeferenced datasets. Table 8. illustrate the Pseudo algorithm for fusing camera images with LiDAR information.



Figure 20. Fused RGB LiDAR data on Camera Pixels

Table 8. Pseudo Algorithm for Fusing Camera Images with LiDAR Information.

<i>Algorithm 3: Fuse Camera Images with LiDAR Data</i>			
	- Initialize:		
		-load camera images	
		-load point cloud data	
	-Pre-process		
		- clean the datasets and remove any noise or inconsistencies.	
	- For each image in the camera Images		
		-For each point in lidar Data	
			- Find corresponding points between the image and LiDAR point cloud
			- If corresponding points found
			-compute the transformation matrix using corresponding points
			- Apply the transformation matrix to all points in the image
			- Georeferenced image using the transformed points
		- Overlay LiDAR data onto the georeferenced image	
		- Save fused image	
	- Return fused images		

7.1.2 Computing Window Size Selection

In this terrain modeling research study, the computing window is defined using coordinates X_{min} , Y_{min} , and X_{max} , Y_{max} extracted from the Lidar fused camera data. With every continuous frame change, as the data collection vehicle advances by 3 meters, the processing window is correspondingly adjusted by the same distance. This strategic adjustment ensures that the most relevant points from the point cloud are selected for ongoing analysis. This approach maintains computational precision and accuracy, leading to a highly detailed model for surface grade analysis. See Figure 21.



Figure 21. Computing Window for Data Frame

7.1.3 Slope Orientation-based Terrain Modeling (SOTM)

The Slope Orientation-based Terrain Modelling (SOTM) algorithm has three key stages. The first stage entails extracting surface points from the point cloud in the computing

window range. These extracted points shape the raw data, laying the foundation for the upcoming terrain profile.

In the algorithm's second stage, computations determine the surface grade from the previously extracted points. This stage involves mathematical operations to calculate the steepness or gradient of the surface at each point. Understanding the rate of change in the terrain's elevation at these points gives a clearer picture of the terrain's overall gradient.

Subsequently, the algorithm applies interpolation techniques in the third stage to create a surface grade profile. This process estimates values between two known values to generate a continuous function, filling in data gaps and smoothing the profile. The result transitions from discrete surface grades to a continuous terrain representation. Figure 22. illustrate the algorithm framework of the SOTM algorithm. The following paragraphs discuss the methodology of slope computation and Inverse Distance Weighting (IDW) interpolation as leveraged in this research study.

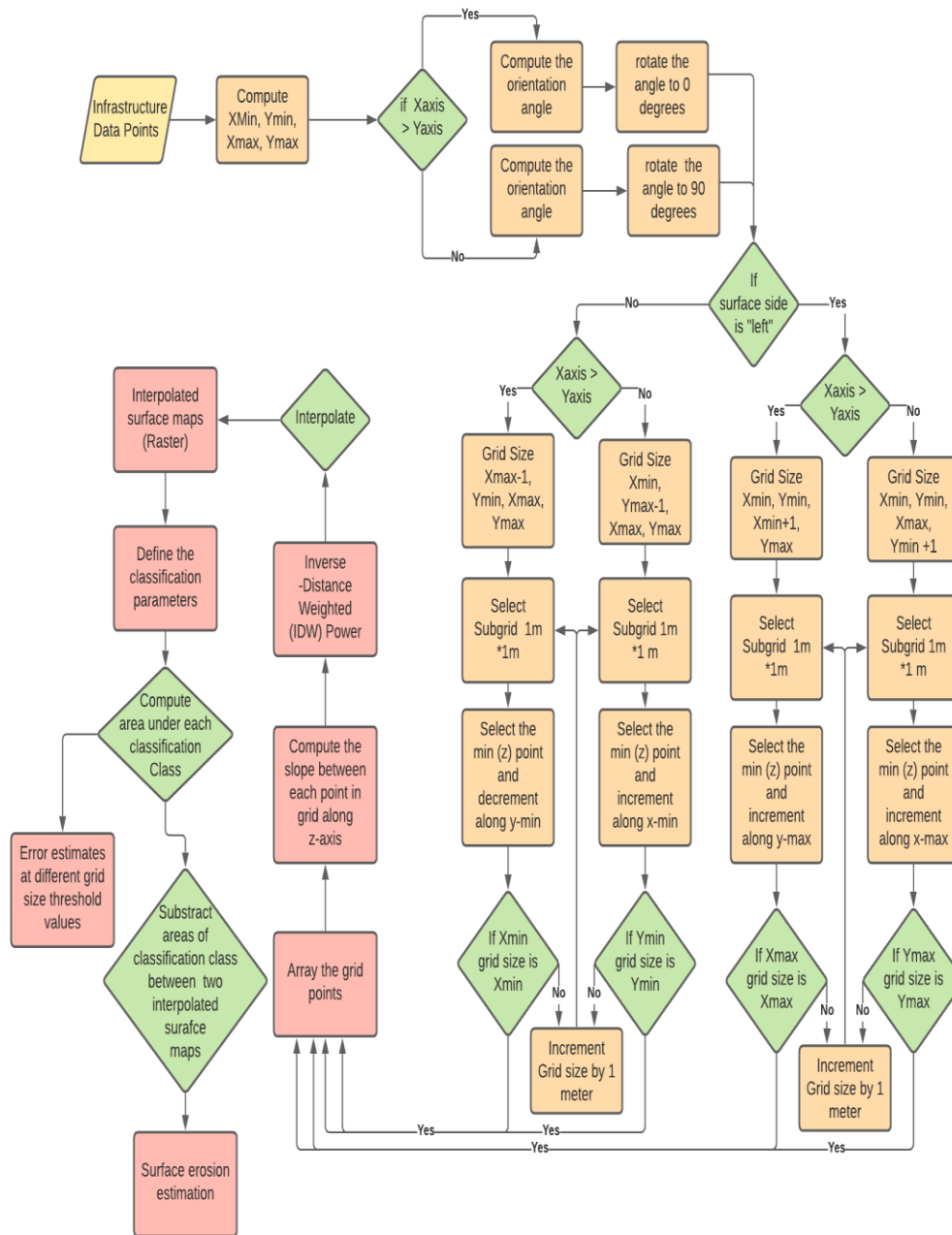


Figure 22. SOTM Algorithm Framework

The slope along the terrain was computed for 5cm wide segments. Each segment was divided into 5cm x 5cm voxel grids. A ground point ($G_1, G_2 \dots G_n$) was randomly selected from each voxel grid. The slope was computed between the selected ground points in voxel

grids ($G_1 - G_2, G_2 - G_3, \dots, G_{n-1} - G_n$) with equation (1) given below, where (x_1, y_1, z_1) are coordinates of the ground point (G_1) and (x_2, y_2, z_2) are coordinates of the ground point (G_2). Slope values were stored in a slope vector (t) { $t_1, t_2, t_3, t_4 \dots t_n$ }, with geo-referenced coordinates. The reference coordinates were increased in 5cm increments before repeating the process. The slope vector values (t) enabled the visual analysis of the surface orientation (e.g., regular or inverted).

$$t_1 = \frac{z_1 - z_2}{\sqrt{(x_1 - x_2)^2 + (y_1 - y_2)^2 + (z_1 - z_2)^2}} \dots \dots \dots (i)$$

Adjacent resulting slope vector values (t) were interpolated to generate the slope terrain map and surface. IDW interpolation was adopted for the analysis because of its accuracy with closely spaced data variables (i.e., < 5 cm in this study) when compared to other interpolation techniques (e.g., Kriging) (Setianto & Triandini, 2013). With variable search radius (z_r), the unknown value (z_t) was computed based on known slope values (i.e. $t_1, t_2, t_3, t_4 \dots t_n$) in the neighborhood with the equation (1) (Bartier and Keller, 1996). Where “ d_i ” was the distance between the known slope value (t_i) and unknown value (z_t), power constant (p) indicates smoothness of surface (default p=2).

$$z_t = \frac{\sum_{i=1}^n \left(\frac{t_i}{d_i^p} \right)}{\sum_{i=1}^n \left(\frac{1}{d_i^p} \right)} \dots \dots \dots (ii)$$

7.2 Visualization

Once the slope grade heat maps are generated leveraging the IDW method. The produced raster files are aligned with the street-level images within the same coordinate system. Due to differing pixel resolutions between the generated heat map and the computing window in the fused dataset, grade maps are displayed in a separate window synchronously with

the moving computing window for enhanced visualization. This process facilitates real-time monitoring of surface grade changes with the change in the data frame.

The surface grade map visually represents the slope pattern in the data frame. See Figure 23. The color spectrum represents slope changes (%) in the embankment. The color spectrum signifies the slope changes (%) in the embankment. Blue color designates positive slope regions, while a gradient from yellow to red marks inverted slope conditions of the terrain surface.

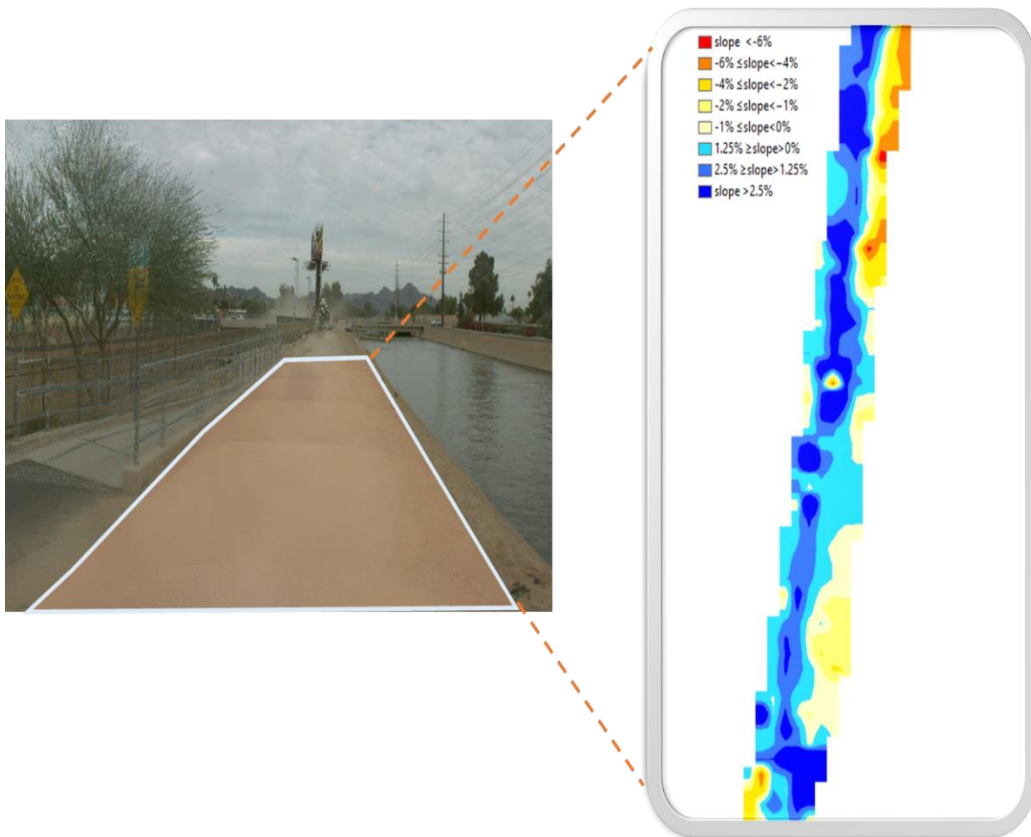


Figure 23. Visualization of Surface Grade Map Integrated with Fusion Dataset.

Furthermore, this research study employed the method for calculating area from pixels under a heat map following the generation of the heat maps. Integral to the process is the

georeferencing phase, where each pixel of the raster image is aligned with LiDAR coordinates, and each pixel of the image. Upon setting these parameters, the computation of the area takes place. Here, this research has specifically computed the area by counting the number of 10cm x 10cm pixels within the same color group on the generated heat map. The quantity of these pixels is multiplied by the area each pixel represents, determined by the spatial resolution. Aggregating these areas yields the total area. The area derived from the color gradient of the slope offers a comparative measure against future datasets for estimating erosion. Table 9. Summarize the results from a data frame shown in Figure 23.

Table 9. Area Under the Terrain Grade Heatmap

Terrain Grade (%)	Area
Slope <-6%	12.9716 m^2
-6% \leq slope <-4%	81.7592 m^2
-4% \leq slope <-2%	106.3896 m^2
-2% \leq slope <-1%	124.7878 m^2
-1% \leq slope < 0%	143.8654 m^2
1.25% \geq slope >0%	258.7318 m^2
2.5% \geq slope >1.25%	176.9864 m^2
Slope > 2.5%	195.5463 m^2
Total Computation Area	1101 m^2

7.3 Limitations

- Dependence on Sensor Accuracy: The quality of the terrain model heavily depends on the precision of the LiDAR and camera sensors. Any inaccuracies in the computing

transformation matrix may impact the fidelity of the generated models, potentially leading to errors in the terrain profile.

- **Homogeneity Assumption:** The method assumes homogeneity in the heat map, with minimal pixel size or shape variations. Any significant distortions or variations in the pixels of the heatmap could impact the accuracy of area calculations.
- **Resolution Limitations:** The granularity of the results is limited by the resolution of the input data. If the spatial resolution is low, fine details of the terrain might not be captured accurately.
- **Static Processing Window:** The processing window remains static at 3 meters increments for every frame change assuming uniformity in computation window size. This might not adequately capture the dynamics of more complex terrains with sharp curves, leading to potential inaccuracies.
- **Error Propagation:** Errors from each stage of the algorithm can propagate to subsequent stages. For instance, any error in point extraction can affect the surface grade calculation and, subsequently, the interpolation process, leading to compounded inaccuracies in the final model.

CHAPTER 8

TREE SPECIES DETECTION AND CLASSIFICATION

The growth of trees and their interaction with powerlines presents a considerable risk to power infrastructure, with potential outcomes ranging from service interruptions to catastrophic events like wildfires. Identifying tree species and understanding their growth patterns can significantly contribute to proactive management, reducing these risks (Ray et al., 2020).

Currently, the maintenance of powerline corridors primarily involves manual labor, which is labor-intensive, costly, and inefficient. An automated, machine-learning-based solution, such as the one proposed in this research, can provide more consistent results faster and at a lower cost. By identifying different tree species, this research can provide valuable insights into each species' unique growth patterns, enabling more accurate predictions about when and where tree pruning might be needed.

This research study revolves around leveraging Mask R-CNN, a deep learning method known for its versatility and performance in instance segmentation tasks (He et al., 2018). Despite the technical challenges associated with "Instance Segmentation for Classification Classes," Mask R-CNN has recently proven its efficacy, becoming the architecture of choice for many researchers. Its robust performance in recent COCO Instance Segmentation challenges further underlines its suitability for this study.

Mask R-CNN, implemented in Python 3.8, Karas =2.5, and TensorFlow=2.5, facilitates detecting and classifying individual tree species within images. The process yields several outputs: bounding boxes around each detected infrastructure object in pixel coordinates, a

probability score assigned to a detected object class, and a pixel mask for each detected object.

Once trained, the Mask R-CNN model can efficiently detect and classify tree species in new, previously unseen images. The training and evaluation strategies are integral components of the research and are discussed in the following paragraphs. Figure 24. illustrates Mask-RCNN architecture.

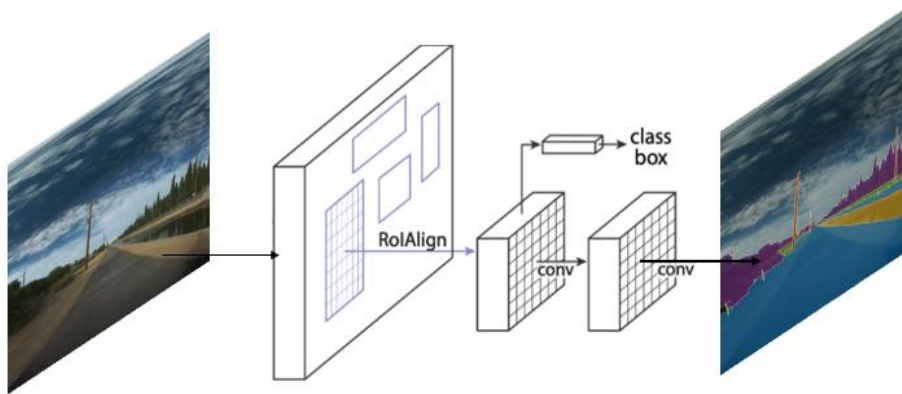


Figure 24. Mask R-CNN Framework

8.1 Mask R-CNN Architecture

In this research, the Mask R-CNN architecture, notable for its proficiency in instance segmentation tasks, is used. This model, an expansion of the Faster R-CNN object detection framework, includes an additional third branch predicting an object mask in parallel with existing branches for bounding box detection and class prediction.

The training of the Mask R-CNN model occurs in two main stages:

- Region Proposal Network (RPN): This study trains a fully convolutional RPN end-to-end, which suggests potential object bounding boxes. It receives an entire image as

input and delivers a set of objects bounding box proposals, each accompanied by an object confidence score.

- **ROI Classifier & Bounding Box Regressor:** The Region of Interest (ROI) pooling layer takes the RPN's proposals and extracts relevant features using the feature map created by the backbone network (ResNet-101). These features assist in predicting the object's class and refining the bounding box coordinates.
- **Segmentation Masks:** The research introduces a third branch running parallel to the existing branches for bounding box recognition and class prediction. It aligns the positive regions derived from the ROI classifier and directs them through a series of convolution layers, finally outputting a binary mask for each class.

The training process involves minimizing a multi-task loss, which is a weighted sum of the classification loss, localization loss (bounding-box regression), and mask loss.

ResNet-101, a deep residual network with 101 layers, is the backbone of the Mask R-CNN architecture employed in this research. ResNet-101 helps to address the vanishing gradient problem, enabling the model to learn more intricate features effectively. As a feature extractor in Mask R-CNN, ResNet-101 accepts the entire image as input. It returns a convolutional feature map, capturing lower-level details (e.g., edges, textures) and higher-level aspects (e.g., shapes). Figure 25. illustrate Mask R-CNN algorithmic workflow for classifying tree species.

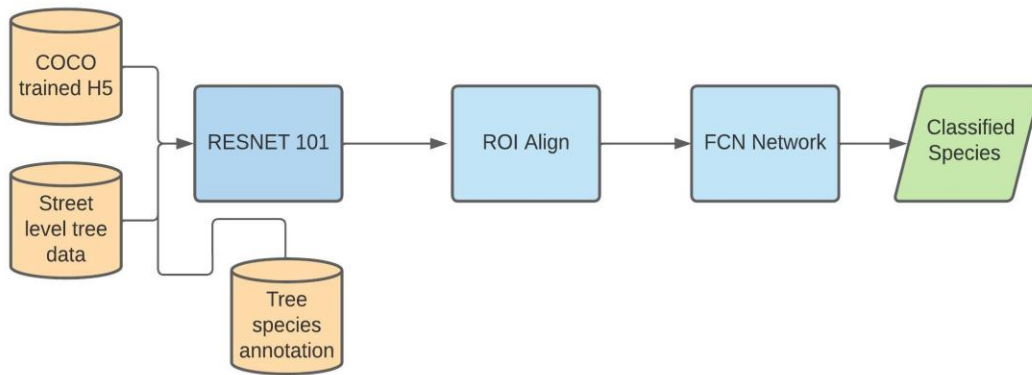


Figure 25. Mask R-CNN Workflow

Once trained, the model can process new images by classifying tree species, providing bounding boxes for the detected trees, and creating pixel masks for each detected object. The outputs from this research provide a comprehensive understanding of tree species distribution in powerline corridors, contributing significantly to strategic infrastructure management.

8.2. Training, Validation, and Testing Datasets

This research leverages the pre-trained Mask R-CNN model, using approximately 36,500 images extracted from the COCO Stuff dataset (Lin et al., 2014). The COCO Stuff dataset, an open-source image library, offers semantic segmentation labels (~164,000) for amorphous classes such as roads, bricks, walls, and trees.

Subsequently, the study fine-tuned the Mask R-CNN model with local Phoenix metropolitan area tree species images. Due to the lack of an open-source dataset suitable for deep neural network (DNN) model training specific to tree species classification, a unique dataset was created. This novel dataset combined images from Google and street-level images, culminating in 500 manually labeled images across five tree species classes,

and all other vegetation in the images were labeled as “others” specie class. The new dataset was then divided into training, validation, and testing datasets in an 8:1:1 ratio. The five species used in the study are shown in Figure 26. Following Table 10. illustrates the pseudo-code for the mask RCNN model.

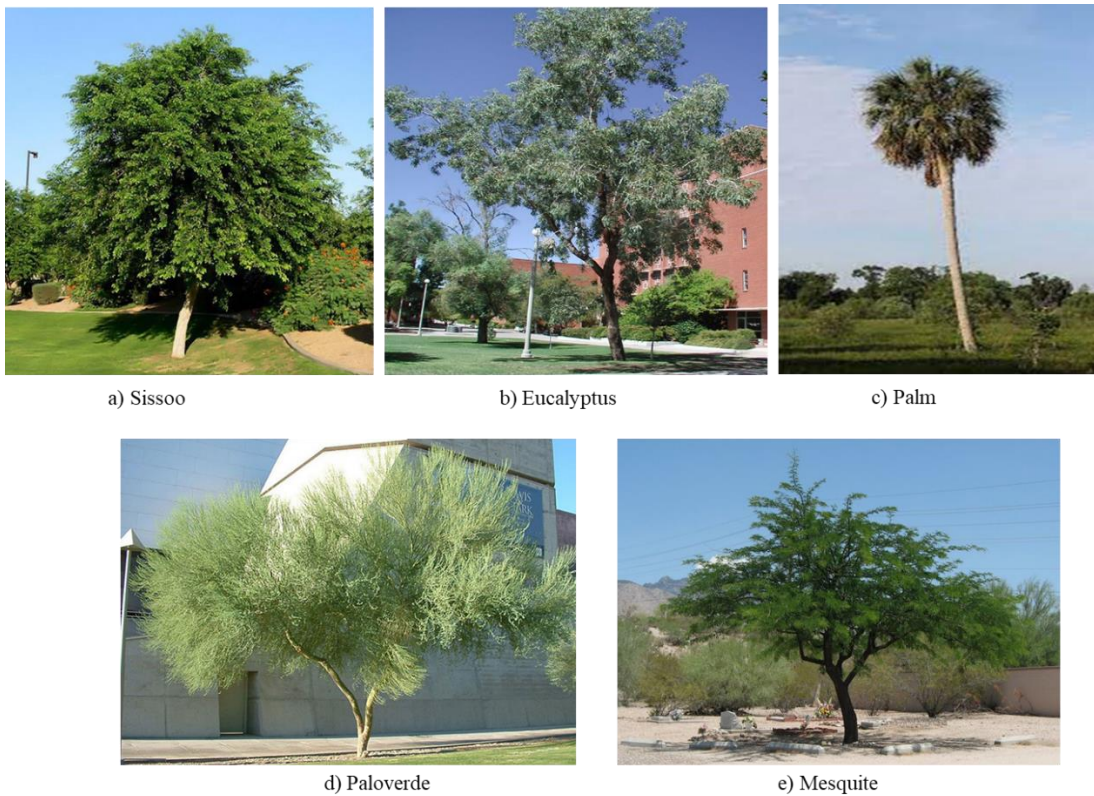


Figure 26. Tree Species Leveraged for Model Training.

Table 10. Pseudo Code for Mask R-CNN Implementation

Algorithm 4: <i>Mask R-CNN Implementation on Custom Build Dataset</i>	
	- Define Mask R-CNN model with ResNet-101 backbone, a Region Proposal Network (RPN), ROI classifier & bounding box regressor, and a segmentation mask.
	- Initialize model parameters.
	- For each epoch in the total number of epochs:
	- Extract features using the ResNet-101 backbone from the input image to generate feature maps.
	- Generate object proposals using the RPN with the feature maps as input
	- Define the regions of interest (ROIs) using the proposals.
	- Classify the object in each ROI and refine its bounding box coordinates using the ROI classifier and bounding box regressor, with the ROIs and feature maps as input.
	- Generate a binary mask for each class using the segmentation mask, with the ROIs and feature maps as input.
	- Compute the losses: RPN classification loss, RPN bounding box loss, ROI classifier loss, ROI bounding box loss, and segmentation mask loss.
	- Combine these losses to get the total loss.
	- Use backpropagation to calculate the gradients of the total loss with respect to the model parameters.
	- Update the model parameters using these gradients.
	- After training, use the trained model to make predictions on new images.

8.3 Proof of Concept

The Mask R-CNN model in this study is trained using a custom dataset of tree species specific to the Phoenix metropolitan area. The data comprises approximately 500 manually labeled images of five distinct tree species. Each image was scrutinized to label individual tree instances using the "Make Sense AI" annotation tool.

After initializing the model parameters, the training process spans 200 epochs, a value determined empirically for satisfactory model performance. Within each epoch, the model goes through feature extraction, region proposal, ROI pooling, and the final task of bounding box regression, class prediction, and binary mask generation. At each step, losses are computed and summed, providing a comprehensive total loss for the system.

Backpropagation then calculates the gradients based on this total loss, and the model parameters are updated accordingly, paving the way for learning from the data. This cycle is repeated for each of the 200 epochs, with the model constantly refining its understanding of the data and improving its predictive capabilities.

During training, the validation dataset, a subset of the overall data, ensures the model's robustness and generalizability. It helps avoid overfitting by checking the model's performance with unseen data.

The study uses a subset of the overall data, the validation dataset, to ensure the model's robustness and generalizability during training. This validation data helps prevent overfitting by actively checking the model's performance against unseen data.

Upon completion of the training process over the defined epochs, the model stands prepared to make predictions on new images. It performs instance segmentation tasks and

identifies tree species, drawing on the knowledge gained from the initial training with the custom dataset.

8.3.1 Results

The model, once trained, is subjected to a test using a new dataset, with the resulting outcomes illustrated below. Five representative images, i.e., Figure 27. Sissoo tree, Figure 28. Eucalyptus tree, Figure 29. Palm tree, Figure 30. Paloverde tree, Figure 31. Mesquite tree demonstrates the model's predictive capabilities, displaying the predicted mask, bounding box, and the accuracy of tree species identification.

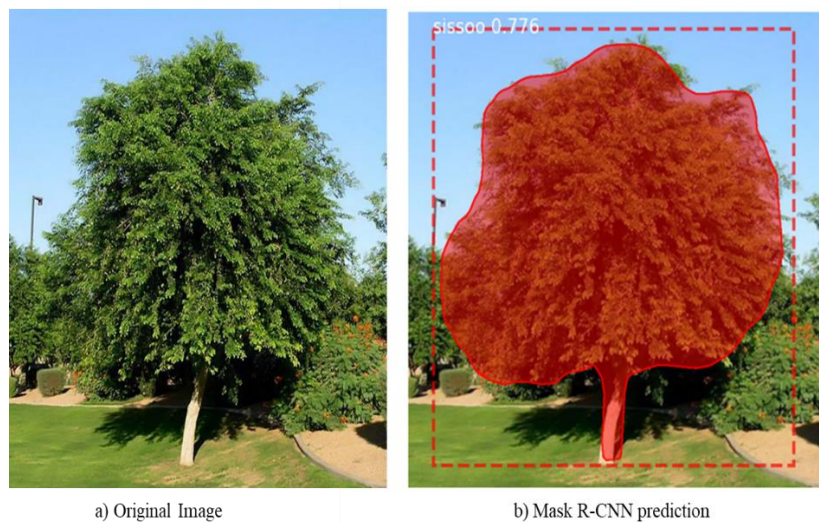


Figure 27. Model Prediction Sissoo Tree, Confidence = 77.6%



a) Original Image

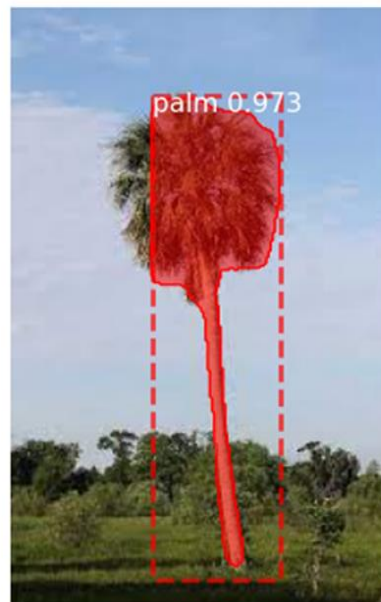


b) Mask R-CNN prediction

Figure 28. Model Prediction Eucalyptus Tree, Confidence = 84.9%



a) Original Image



b) Mask R-CNN prediction

Figure 29. Model Prediction Palm Tree, Confidence = 97.3%

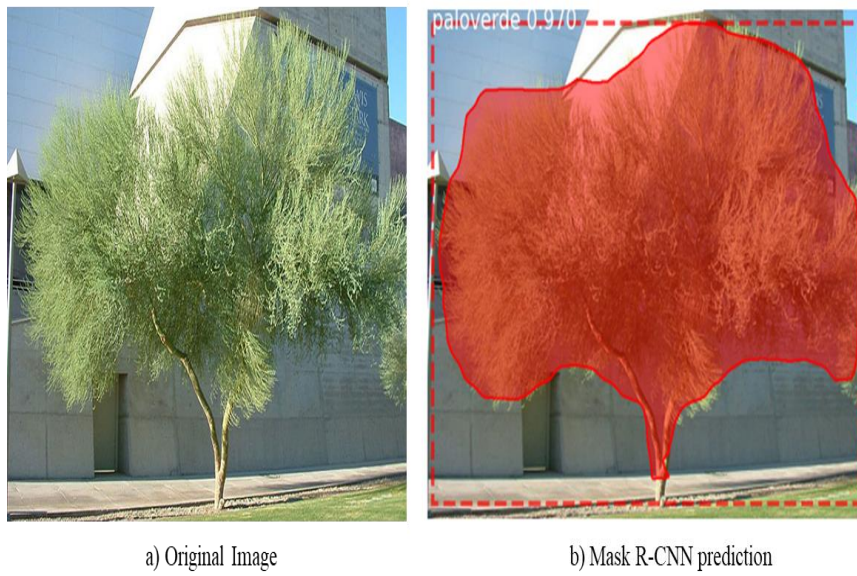


Figure 30. Model Prediction Paloverde Tree, Confidence = 97.0%

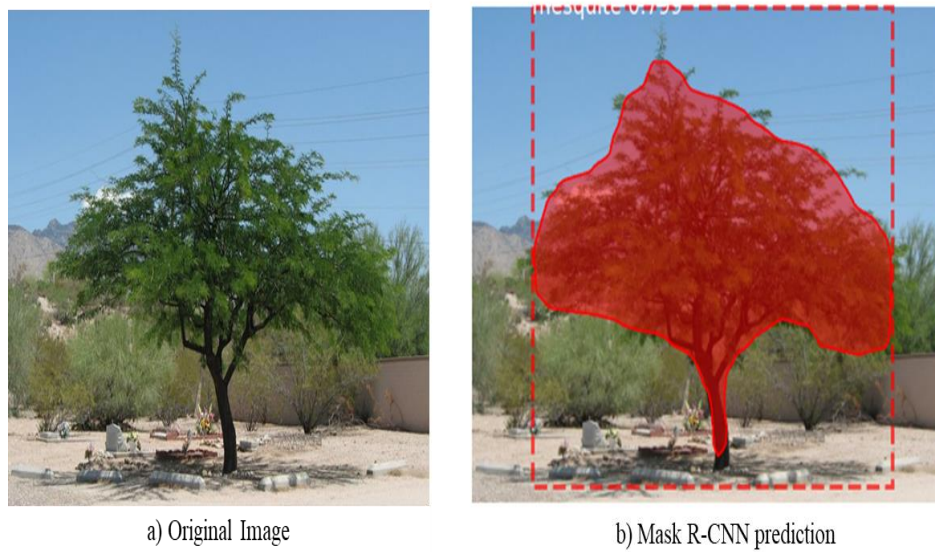


Figure 31. Model Prediction Mesquite Tree, confidence = 79.9%

The model demonstrates varying degrees of confidence in its five different tree species predictions. For the Sissoo tree, the model reports a prediction confidence of 77.6%, suggesting a moderate level of certainty. In the case of the Eucalyptus tree, the confidence level rises to 84.9%, indicating a higher degree of prediction assurance. The highest confidence levels are reported for the Palm tree and the Palo Verde, standing at 97.3% and 97.0%, respectively, suggesting an exceptional model performance for these species. The Mesquite tree, with a prediction confidence of 79.9%, also showcases a robust prediction capability. These results confirm the model's substantial efficacy in distinguishing and correctly identifying these five tree species.

The following section presents the graphical representation of loss values observed during the model's training. These loss graphs, often referred to as learning curves, play a crucial role in understanding and analyzing the performance and learning progression of the model over time.

The loss graphs typically display two main types of losses: training loss and validation loss, which should ideally decrease throughout training. The training loss represents the model's performance on the data it learns from, while the validation loss shows how well the model generalizes to new, unseen data.

Significant aspects to observe in these graphs include the overall trend of loss reduction and the potential existence of overfitting or underfitting. Overfitting occurs when the training loss continues to decrease significantly (to “zero”), but the validation loss increases, indicating that the model is memorizing the training data but performing poorly

on new data. Conversely, underfitting happens when both losses remain high, indicating that the model is not learning adequately from the training data.

By monitoring these loss graphs, important insights about the model's learning process can be extracted, further, adjust the training parameters if necessary, and ultimately guide the model toward better performance. The goal is to have both the training and validation losses decrease to a point of stability with a minimal gap between them. The following log graphs offer insights into the training and validation results for 200 epochs on a tree species dataset trained with the Mask R-CNN model, revealing key patterns and trends that aid in understanding the model's learning dynamics. Refer to Figures 32-44.

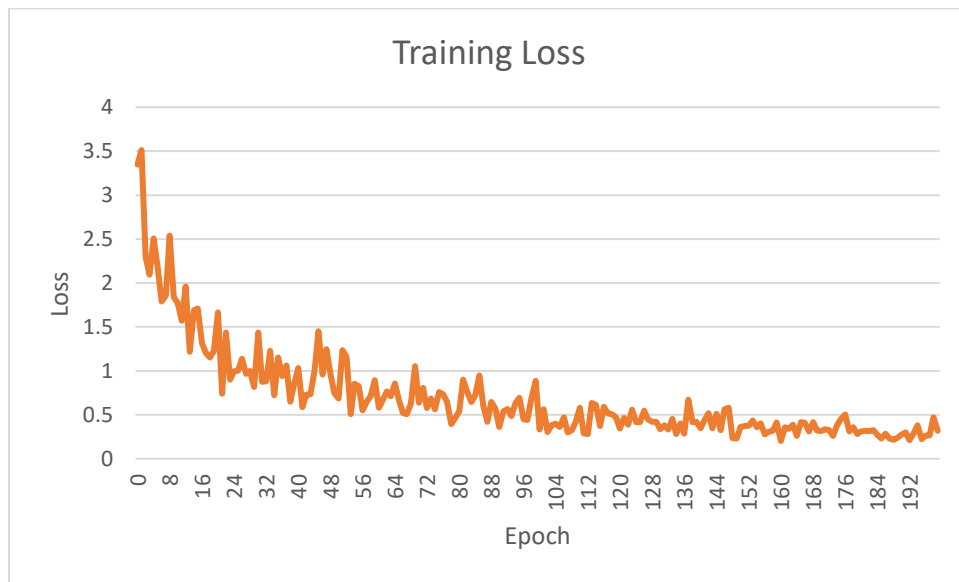


Figure 32. Tree Species Dataset -Training Loss Curve

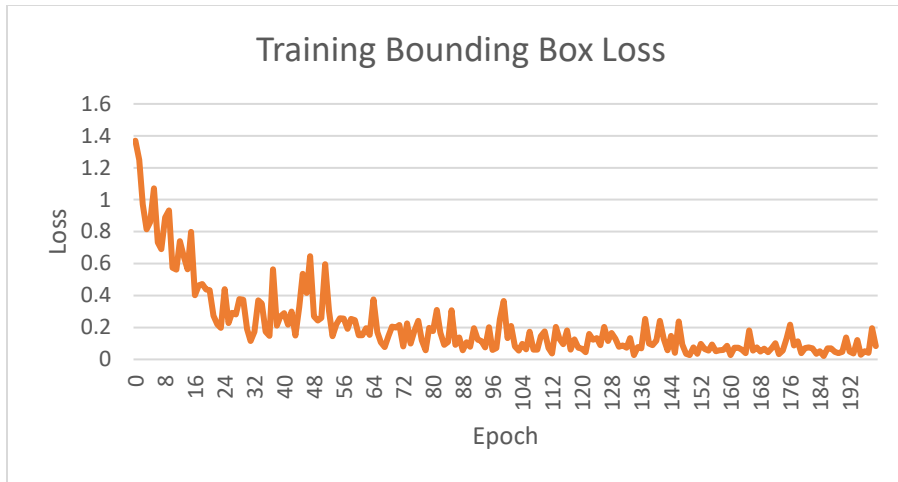


Figure 33. Tree Species Dataset -Training Bounding Box Loss Curve

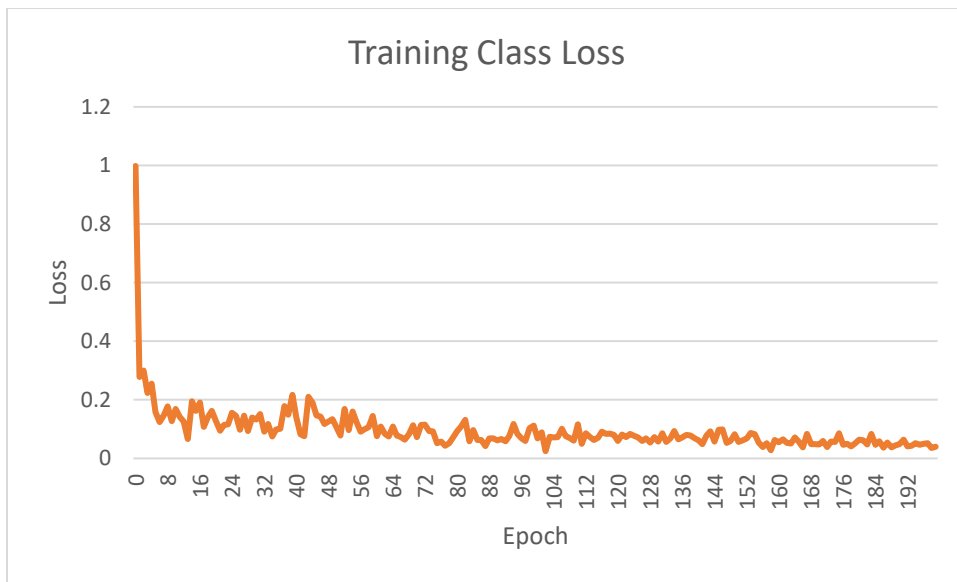


Figure 34. Tree Species Dataset -Training Class Loss Curve

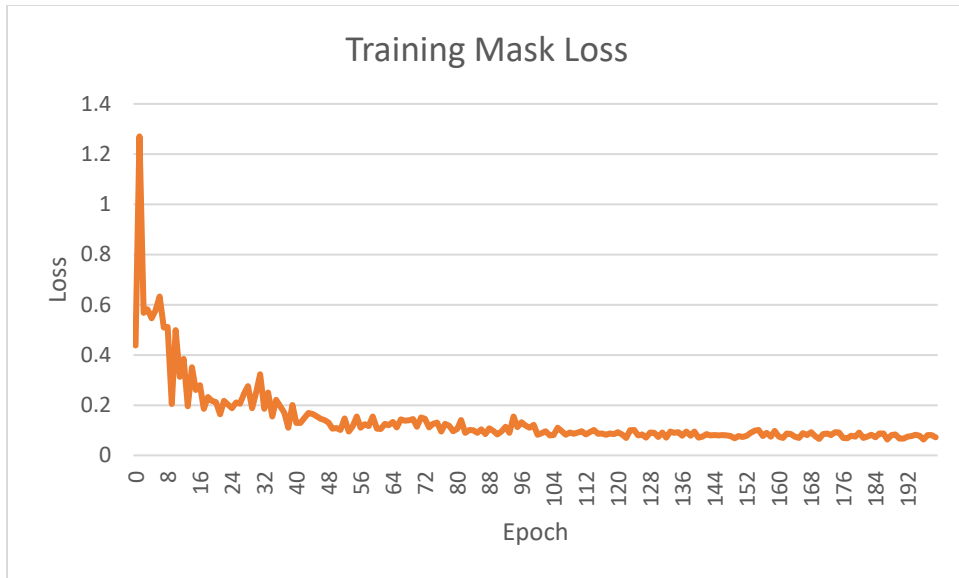


Figure 35. Tree Species Dataset -Training Mask Loss Curve

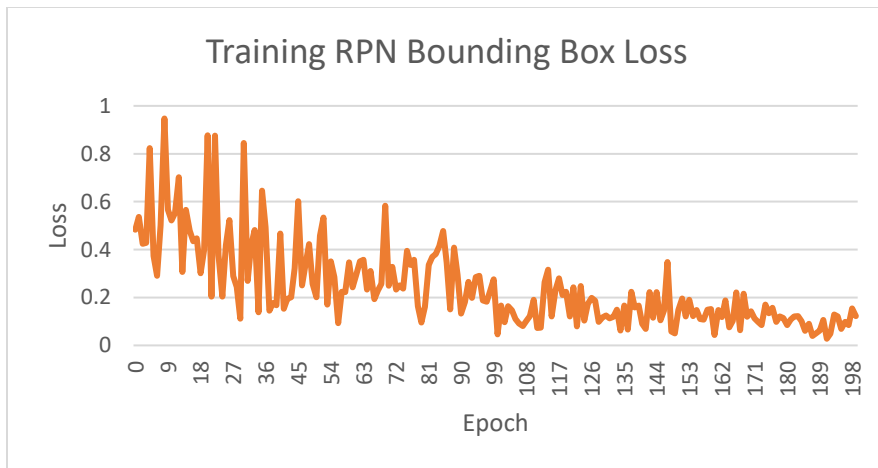


Figure 36. Tree Species Dataset -Training RPN BBox Loss

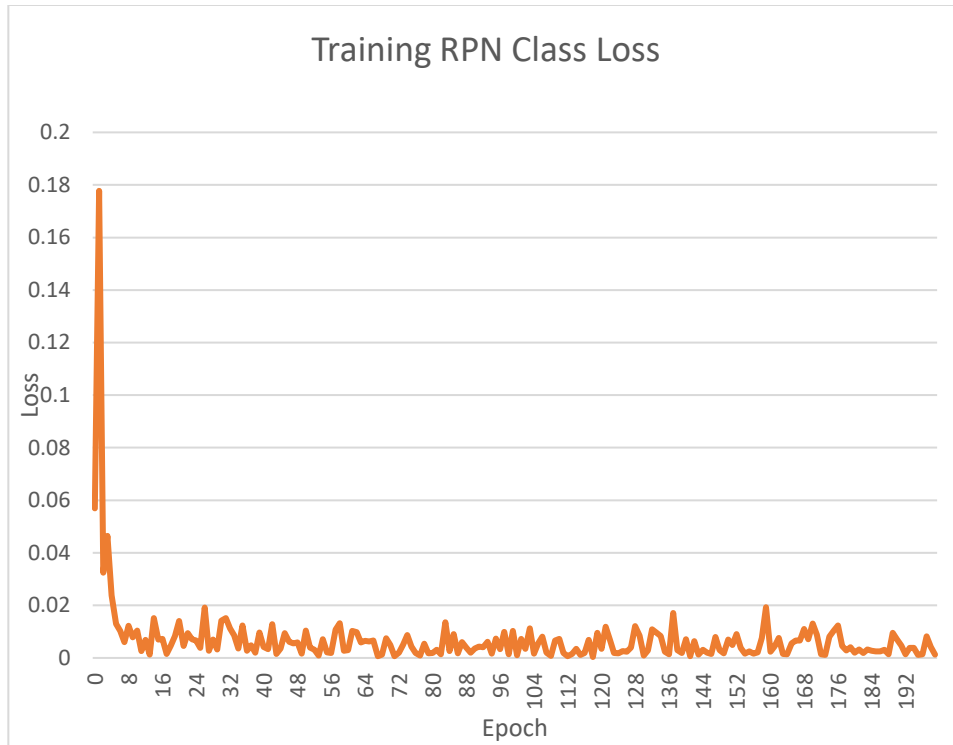


Figure 37. Tree Species Dataset -Training RPN Class Loss

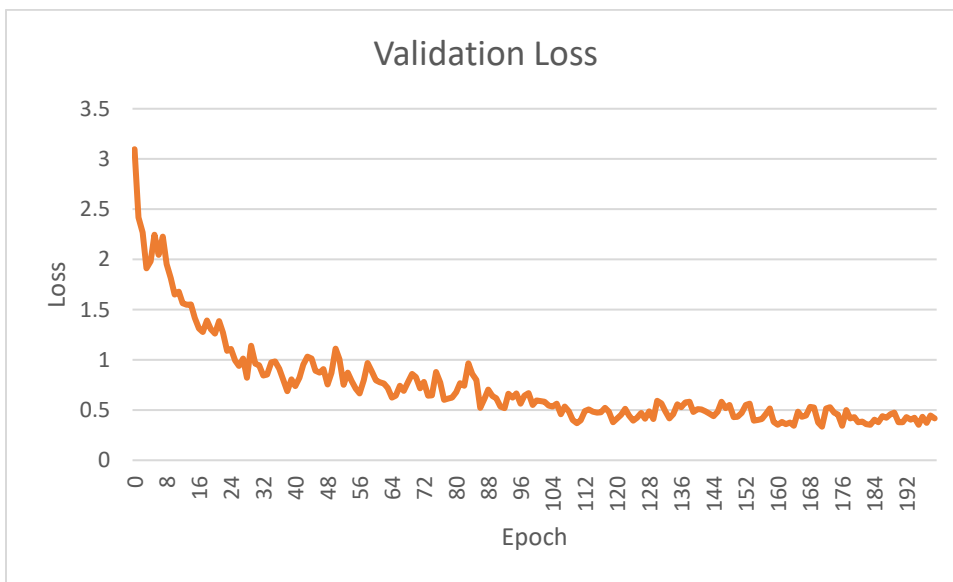


Figure 38. Tree Species Dataset -Validation Loss

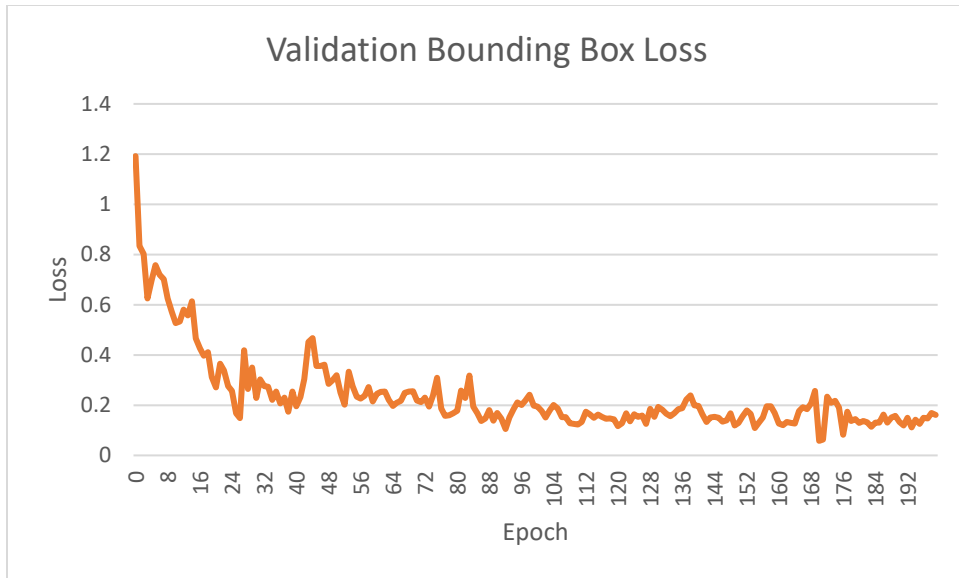


Figure 39. Tree Species Dataset -Validation BBox Loss

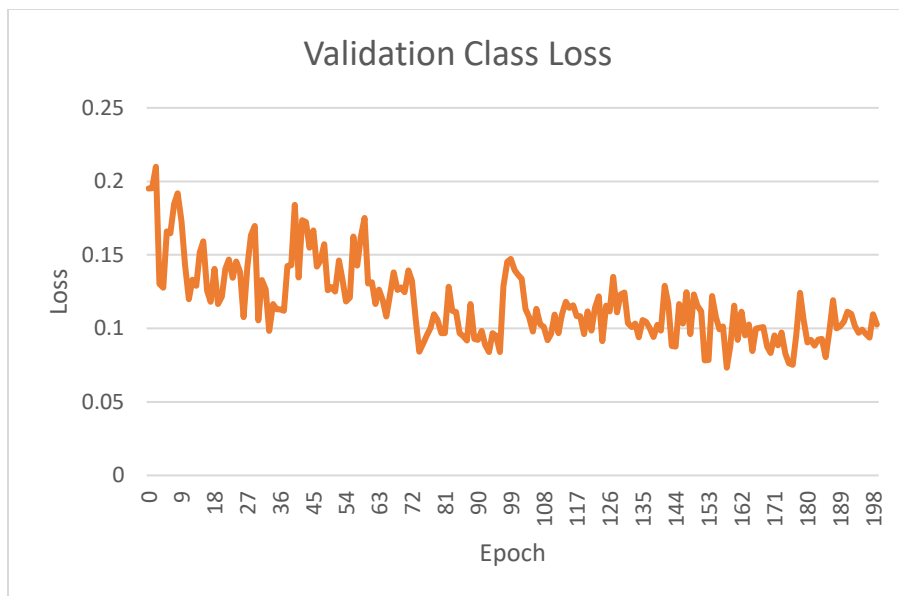


Figure 40. Tree Species Dataset -Validation Class Loss

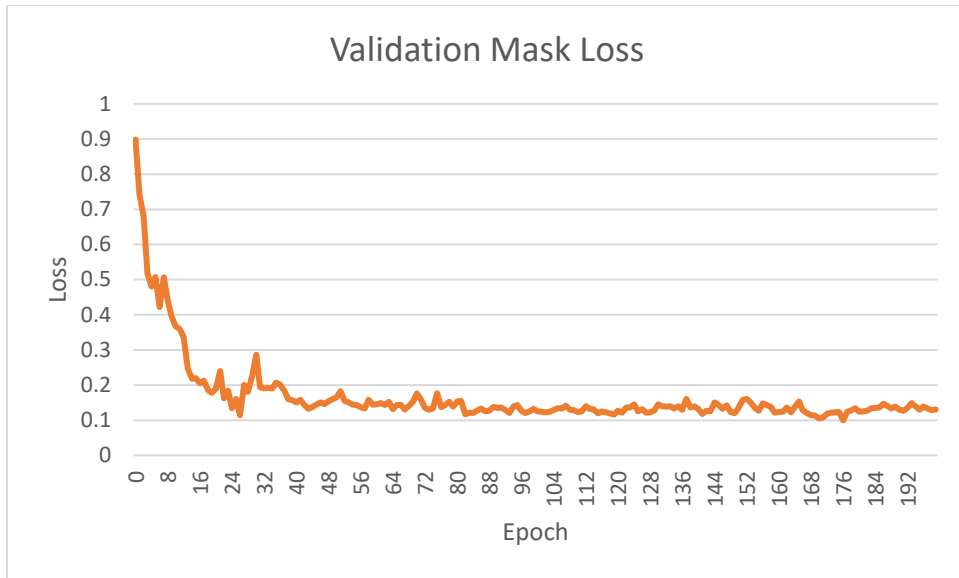


Figure 41. Tree Species Dataset -Validation Mask Loss

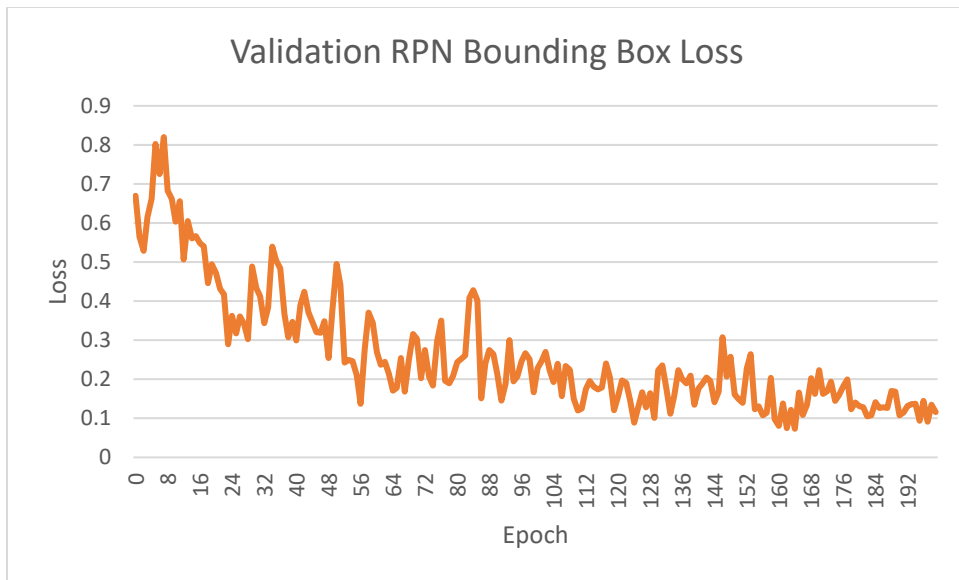


Figure 42. Tree Species Dataset -Validation RPN Bounding Box Loss

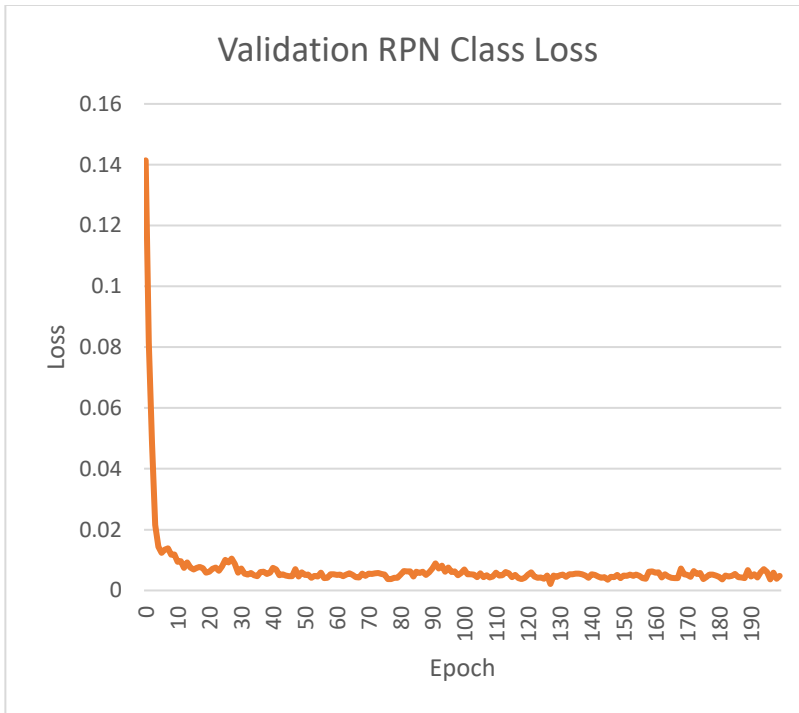


Figure 43. Tree Species Dataset -Validation RPN Class Loss

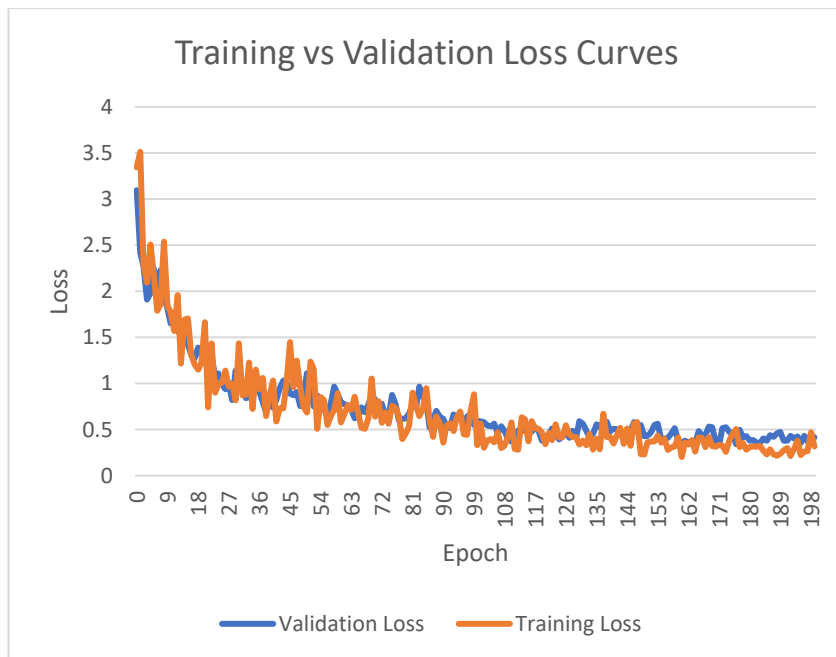


Figure 44. Loss Curves for Tree Species Dataset

The alignment of the training and validation loss curves in the presented graphs indicates a strong model performance. This alignment suggests that the model is successfully generalizing from the training data to unseen data, a critical factor in assessing model accuracy. It implies a low bias and variance trade-off, reducing the likelihood of overfitting or underfitting.

In conclusion, given the close alignment of the loss curves and the high confidence levels in tree species identification, it can be inferred that the model has achieved a high level of accuracy. This robust performance validates the efficacy of using the Mask R-CNN model with a ResNet-101 backbone for tree species identification tasks.

Furthermore, in this research study, comparison graphs were generated to evaluate the accuracy of the tree species classification against the ground truth from the testing dataset. A thorough analysis of these graphs reveals the model's success and challenges in distinguishing between tree species. Specifically, the model demonstrated an accuracy of 71% in detecting mesquite trees. However, 23% of mesquite trees were incorrectly classified as other vegetation types. Interestingly, the model also misclassified 5% of mesquite trees as paloverdes. Refer to Figure 45.

Paloverde trees, on the other hand, showed a classification accuracy of 73% with the model, while 16% were wrongly identified as other tree types. Additionally, the model misclassified 10% of paloverdes as mesquites. Refer to Figure 46. In stark contrast, the model exhibited exceptional performance in identifying palm trees, with an accuracy rate of 99%. Refer to Figure 47.

As for the classification of eucalyptus and sissoo trees, the trained model demonstrated substantial proficiency with 86% and 85% accuracy rates, respectively. Refer to Figure 48 & Figure 49. Overall, these findings underscore the trained model's capabilities and limitations in identifying and differentiating between various tree species.

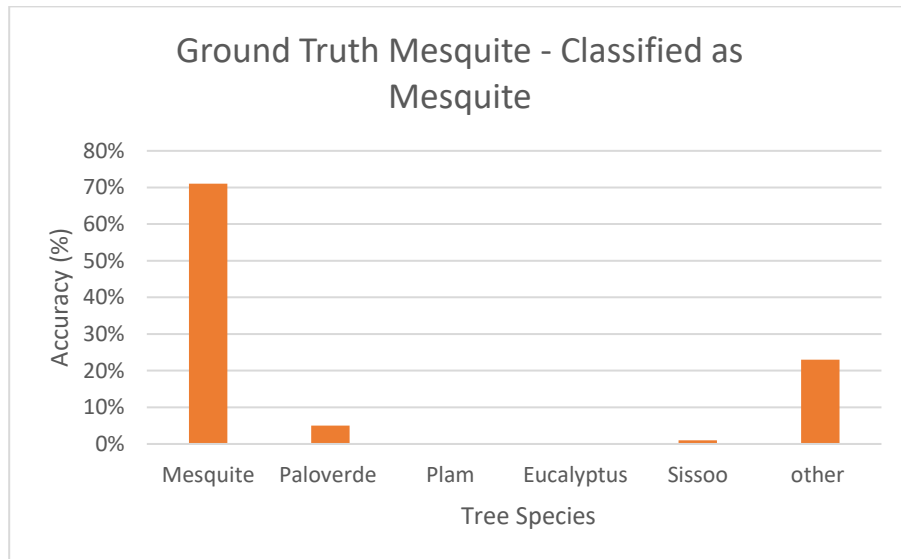


Figure 45. Accuracy on Testing Dataset – Mesquite Trees

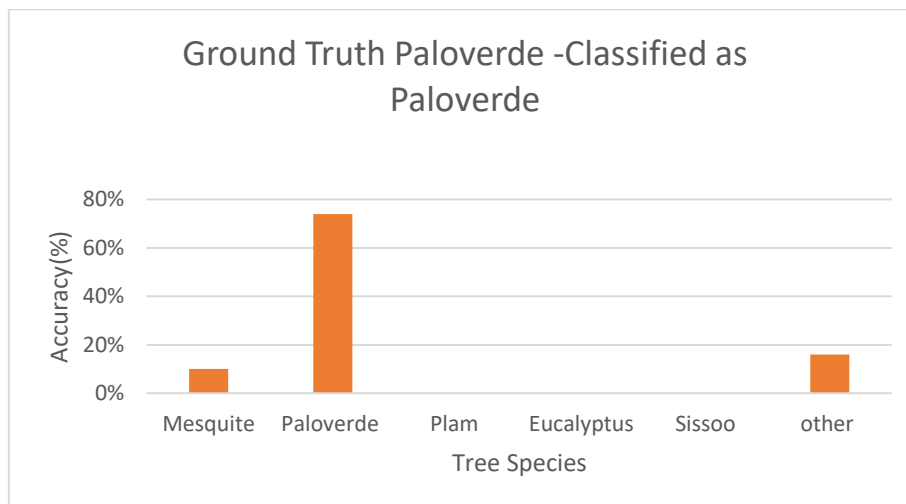


Figure 46. Accuracy on Testing Dataset – Paloverde Trees

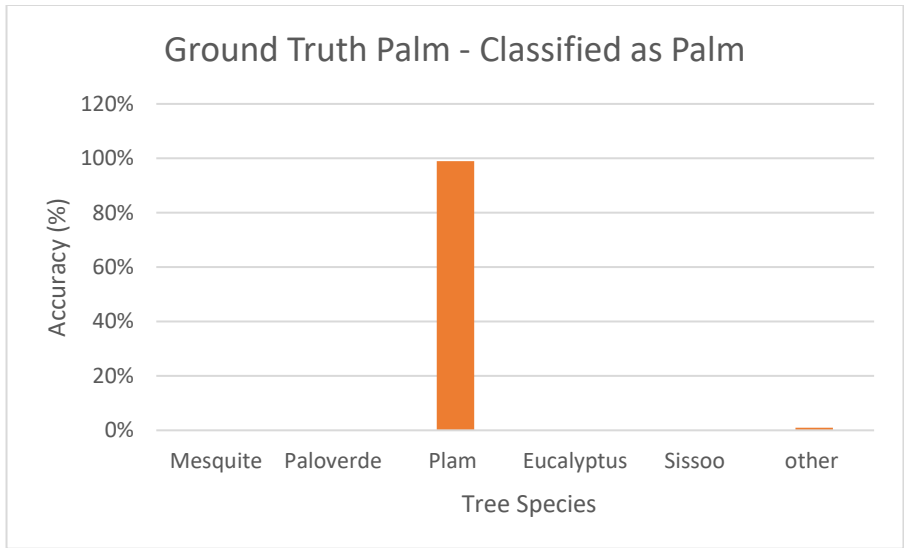


Figure 47. Accuracy on Testing Dataset – Palm Trees

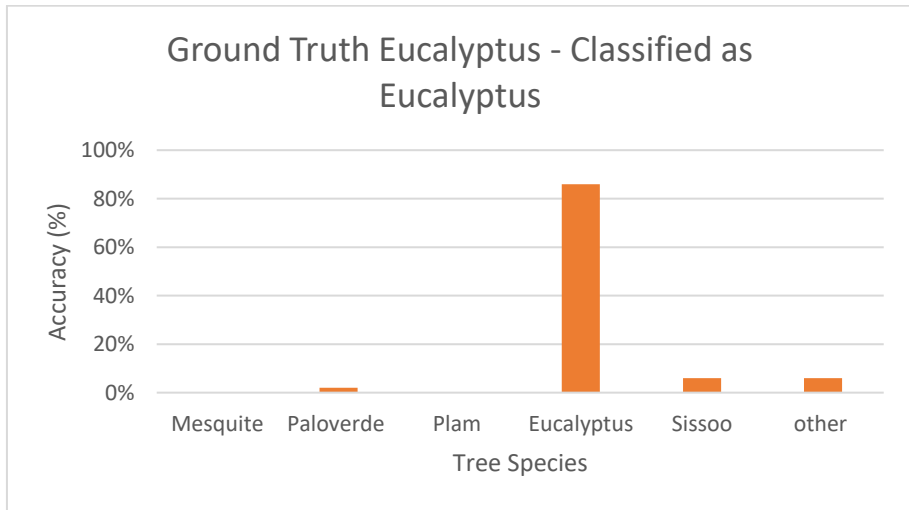


Figure 48. Accuracy on Testing Dataset – Eucalyptus Trees



Figure 49. Accuracy on Testing Dataset – Sissoo Trees

8.4 Limitations

Although the model demonstrates considerable accuracy and robust performance, certain limitations should be acknowledged.

- **Data Quantity:** Although a substantial effort was made to collect and label a diverse set of images for training, the number of images and the variety of tree species might not fully represent all scenarios in a real-world setting.
- **Image Quality:** The model's performance is directly influenced by the quality and clarity of the images. Factors such as lighting conditions, camera angle, resolution, and occlusions may impact the model's ability to classify and locate trees accurately.
- **Generalization:** The model may not generalize to regions with unique trees, environmental conditions, or species not included in the training data. This includes different growth stages, tree health conditions, or variations in shape and size.

CHAPTER 9

CONCLUSION

This research paper has applied artificial intelligence models to address critical infrastructure operations and maintenance. The study focused on point cloud noise processing using neural networks, automated tree species detection using Mask R-CNN, and real-time terrain analysis by combining image and LiDAR datasets. The overall goal of this research was to leverage artificial intelligence to support the maintenance and upkeep of aging large civil infrastructure, with the ultimate objective of ensuring a sustained state of repair and functionality.

The findings of this study have yielded significant contributions to the field. Firstly, the implementation of neural networks for point cloud noise processing has demonstrated its potential in effectively eliminating unwanted noise, thus enhancing the accuracy and reliability of infrastructure data. This provides a means to improve the quality and integrity of monitoring data, leading to better-informed decision-making processes and more precise maintenance interventions.

Secondly, integrating Mask R-CNN for automated tree species detection presents a valuable solution for efficiently identifying and classifying vegetation surrounding infrastructure. By accurately identifying tree species, infrastructure managers can proactively plan and execute vegetation management strategies, reducing risks associated with tree-related incidents and ensuring the safety and longevity of infrastructure assets.

Lastly, the fusion of image and LiDAR datasets for real-time terrain analysis offers a comprehensive understanding of the terrain's characteristics and potential hazards. This

integrated approach enables infrastructure managers to assess slope, elevation, and other relevant factors, facilitating proactive maintenance interventions and mitigating risks associated with terrain-related issues.

Collectively, the outcomes of this research underscore the crucial role that artificial intelligence models play in advancing the operations and maintenance practices of aging large civil infrastructure systems. By leveraging the power of AI, infrastructure managers can optimize their decision-making processes, streamline maintenance efforts, and promote the overall health and resilience of vital infrastructure networks. The findings presented in this study pave the way for enhanced infrastructure management strategies and contribute to the collective efforts to maintain a robust and reliable infrastructure system to benefit society.

In addition to the specific contributions mentioned above, this research paper holds broader implications for infrastructure management. By harnessing the capabilities of artificial intelligence models, the study has demonstrated the potential to overcome longstanding challenges associated with complex large infrastructure systems. The ability to process point cloud noise, detect tree species, and analyze terrain in real-time improves the efficiency and accuracy of maintenance efforts and enables proactive decision-making and resource allocation. This proactive approach to infrastructure management is crucial in ensuring the longevity and functionality of critical civil infrastructure, especially in the face of increasing demands and aging systems.

Furthermore, the research highlights artificial intelligence's transformative role in infrastructure operations and maintenance. Traditionally, these tasks have relied on manual

inspection, subjective assessments, and limited resources. However, integrating AI models and advanced sensing technologies offers a paradigm shift in monitoring and maintaining infrastructure. The automation and intelligence brought by these models streamline processes, reduce human error, and enhance the overall effectiveness of maintenance activities. As a result, infrastructure managers are better equipped to optimize resources, minimize downtime, and prioritize maintenance efforts based on accurate and real-time insights, ultimately leading to improved infrastructure performance and resilience.

In conclusion, the findings presented in this research paper underscore the significant potential of artificial intelligence models in supporting the operations and maintenance of large infrastructure systems. The application of neural networks for point cloud noise processing, automated tree species detection using Mask R-CNN, and real-time terrain analysis through image and LiDAR fusion offer valuable solutions to address challenges in infrastructure management. By leveraging these advancements, infrastructure managers can make informed decisions, enhance maintenance strategies, and ensure the longevity and reliability of vital infrastructure systems. The research opens new avenues for further exploration and underscores the importance of embracing AI-driven approaches to maximize the performance and sustainability of our infrastructure networks.

CHAPTER 10

BROADER IMPACTS

The proposed methodology has the potential to provide managers/engineers/concerned local authorities with the necessary information to make informed decisions regarding the operation and maintenance of large infrastructure systems. Some of the impact benefits of the proposed methodology are as follows:

- The research will contribute to more accurate and reliable data analysis across various fields, including remote sensing, computer vision, and autonomous systems. The successful implementation of O&M tasks may lead to the creation of new job opportunities in the field, promoting U.S. economic growth.
- Optimized O&M activities through digitization and advanced computing promises to improve/extend the life span of infrastructure systems, reducing the frequency and cost of major reconstruction. This would ultimately reduce the cost burden on U.S. local authorities.
- Real-time analysis and optimized O&M will contribute to data-driven decision-making, ensuring that resources are allocated efficiently and effectively to identify potential hazards, leading to quicker interventions, and ultimately enhancing the safety of U.S. society by mitigating catastrophic infrastructure failures.
- Real-time analysis and optimized O&M promises to improve transportation systems by reducing the occurrence of potholes, cracks, and other surface issues, which can promote economic growth and save billions of dollars for U.S. society by enhancing connectivity, and reduce travel times, wasted fuel, and vehicle maintenance.

- The research will contribute to more effective vegetation management around critical infrastructure, such as power lines and transportation networks. This will help prevent power breakouts caused by the intrusion of vegetation growth, ensure the safety of maintenance personnel, and enhance better decision-making for O&M activities.
- This research will contribute to developing comprehensive and integrated O&M solutions. These solutions can leverage cutting-edge technologies, such as artificial intelligence, Internet of Things (IoT), augmented reality (AR), virtual reality (VR), and mixed reality (MR) applications to streamline O&M processes, reduce cost, mitigates risk, ultimately leads to safer, more sustainable infrastructure systems, and enhanced infrastructure resilience.

CHAPTER 11

INTELLECTUAL MERIT

The intellectual merit of this research lies in addressing the existing limitations. It aims to adopt analytical models for processing large point cloud datasets, which are critical to understanding and managing complex civil infrastructure systems. The research aims to significantly improve the accuracy and efficiency of automated feature extraction from point cloud and imagery data by developing novel analytical models and incorporating deep learning techniques.

- The proposed method provides a more efficient and effective way to filter noise and extract infrastructure surface points than existing algorithms.
- The research enhances tree species classification using deep learning models to accurately classify and distinguish overlapping tree species by effectively interpreting the complex contextual information from natural environments.
- The proposed robust real-time analytics for terrain assessment for surface grade and erosion estimation enables accurate, efficient, and rapid terrain analysis, outperforming the traditional geometric methods.
- The proposed real-time fusion method overcomes the pre-processing requirement while analyzing the terrain information from the point cloud dataset with heavy noise acquired from complex reflective environments.

REFERENCES

- American Society of Civil Engineers (ASCE). (2012-2021). Failure to Act: Closing the Infrastructure Investment Gap for America's Economic Future. Retrieved from
- American Society of Civil Engineers (ASCE). (1998-2021). Infrastructure Report Card. Retrieved from <https://www.infrastructurereportcard.org>
- National Council on Public Works Improvement (NCPWI). (1988). Fragile Foundations: A Report on America's Public Works. Washington, D.C.: U.S. Government Printing Office.
- Federal Highway Administration. (2019). 2017 Urban Congestion Trends. U.S. Department of Transportation.
- National Transportation Safety Board (NTSB). (2008). Collapse of I-35W Highway Bridge, Minneapolis, Minnesota, August 1, 2007. Accident Report NTSB/HAR-08/03. Retrieved from <https://www.nts.gov/investigations/AccidentReports/Reports/HAR0803.pdf>
- United States Environmental Protection Agency (EPA). (2018). Flint, Michigan Drinking Water Response. Retrieved from <https://www.epa.gov/flint>
- Los Angeles Department of Water and Power (LADWP). (2014). Update on Water Main Break on Sunset Blvd. Retrieved from <https://www.ladwpnews.com/update-on-water-main-break-on-sunset-blvd/>
- U.S.-Canada Power System Outage Task Force. (2004). Final Report on the August 14, 2003 Blackout in the United States and Canada: Causes and Recommendations. Retrieved from <https://www.energy.gov/sites/prod/files/oeprod/DocumentsandMedia/BlackoutFinal-Web.pdf>
- Halfawy, M., Newton, L., & Vanier, D. (2002). Integration of municipal infrastructure asset management processes: challenges and solutions. *Journal of Computing in Civil Engineering*, 16(3), 217-229. [https://doi.org/10.1061/\(ASCE\)0887-3801\(2002\)16:3\(217\)](https://doi.org/10.1061/(ASCE)0887-3801(2002)16:3(217))
- World Economic Forum (WEF). (2014). Strategic Infrastructure Steps to Operate and Maintain Infrastructure Efficiently and Effectively. Retrieved from http://www3.weforum.org/docs/WEF_IU_StrategicInfrastructure_Report_2014.pdf
- Achanta, S., Anumba, C. J., Asadi, S., Fonseca, A. S., Giretti, A., Kamsu-Foguem, B., & Wang, J. (2012). A review of process visualization techniques for civil engineering projects. *Visualization in Engineering*, 1(1), 1-14. <https://doi.org/10.1186/2213-7459-1-5>

Johnson, R., Anderson, M., & Miller, G. (2015). Real-time data collection and condition monitoring of large civil infrastructures using sensors and radio-frequency devices. *Journal of Infrastructure Systems*, 21(4), 215-223.

Smith, J., & Brown, D. (2016). Enhancing safety, efficiency, and reliability in civil infrastructures with strain gauges and accelerometers. *Sensors and Actuators for Infrastructure Applications*, 27(6), 789-798.

Williams, T. (2017). RFID tags in civil infrastructure monitoring: A comprehensive review. *Journal of Radio Frequency Identification*, 3(2), 112-128.

Stajano, F., Hault, N., Wassell, I., Bennett, P., Middleton, C., & Soga, K. (2010). Smart Bridges, Smart Tunnels: Transforming Wireless Sensor Networks from Research Prototypes into Robust Engineering Infrastructure. *Ad Hoc Networks*, 8(8), 872-888. <https://doi.org/10.1016/j.adhoc.2010.04.002>

Wu, Chao, Yongbo Yuan, Yang Tang, and Boquan Tian. 2022. "Application of Terrestrial Laser Scanning (TLS) in the Architecture, Engineering and Construction (AEC) Industry" *Sensors* 22, no. 1: 265.

Gupta, P., & Way, T. R. (2010). A review on terrestrial laser scanning for change detection and deformation monitoring of structures. *ISPRS Journal of Photogrammetry and Remote Sensing*, 65(2), 117-130.

Chen, Q. (2007). Airborne lidar data processing and information extraction. *Photogrammetric Engineering and Remote Sensing*, 73(2), 109–112.

Qiao W, Ma B, Liu Q, Wu X, Li G. Computer Vision-Based Bridge Damage Detection Using Deep Convolutional Networks with Expectation Maximum Attention Module. *Sensors (Basel)*. 2021

Wu, W., Li, Y., Tian, Y., Zhang, S., & Xu, Q. (2020). A deep learning-based approach for mapping urban infrastructure from 3D point clouds. *Remote Sensing*, 12(2), 233.

Geng, Liying, Tao Che, Xufeng Wang, and Haibo Wang. 2019. "Detecting Spatiotemporal Changes in Vegetation with the BFAST Model in the Qilian Mountain Region during 2000–2017" *Remote Sensing* 11, no. 2: 103.

del Río-Barral, Pablo, Mario Soilán, Silvia María González-Collazo, and Pedro Arias. 2022. "Pavement Crack Detection and Clustering via Region-Growing Algorithm from 3D MLS Point Clouds" *Remote Sensing* 14, no. 22: 5866.

Chu Chu, Linbing Wang, Haocheng Xiong. 2022. A review on pavement distress and structural defects detection and quantification technologies using imaging approaches, *Journal of Traffic and Transportation Engineering (English Edition)*, Volume 9, Issue 2, Pages 135-150.

- Coren, F., & Sterzai, M. (2006). Monitoring land-cover changes in urban areas with remote sensing: Emphasis on the contribution of LiDAR. *International Journal of Remote Sensing*, 27(10), 1895-1916.
- Giridharan, R., Lau, K. K., & Ganesan, S. (2004). Comparison of urban heat island intensity between a coastal and inland city in Southeast Asia. *Atmospheric Environment*, 38(9), 1359-1366.
- Hecht, R., Trommler, M., & Schenk, A. (2008). Fusion of lidar and hyperspectral data for urban mapping. *ISPRS Journal of Photogrammetry and Remote Sensing*, 63(4), 365-382.
- Höfle, B., & Pfeifer, N. (2007). Correction of laser scanning intensity data: Data and model-driven approaches. *ISPRS Journal of Photogrammetry and Remote Sensing*, 62(5), 415-433.
- Huang, C., Chen, C., Gong, P., & Chen, L. (2013). Comparison of object-based and pixel-based classifications for mapping urban land use/cover using SPOT-5 imagery. *Remote Sensing of Environment*, 134, 210-225.
- Kakon, N. A., Hasan, M. R., & Amin, M. N. (2009). Remote sensing and GIS application for land-use/land-cover change detection analysis in Dhaka Metropolitan, Bangladesh. *Journal of Environmental Science and Technology*, 2(1), 1-8.
- Kotthaus, S., & Grimmond, C. S. (2014). Surface urban heat island gradients across a coastal city and impact on surrounding sea breeze circulation. *Atmospheric Environment*, 99, 296-306.
- Samal, A., & Gedam, S. S. (2015). Extraction of urban features from high-resolution satellite imagery using an object-oriented approach. *International Journal of Remote Sensing*, 36(2), 464-479.
- Zhang, X., Hu, Z., Li, W., Zhang, L., & Li, D. (2008). Distinguishing building footprint information from LIDAR datasets from urban areas. *International Journal of Remote Sensing*, 29(8), 2189-2204.
- Zhang, W., Qi, J., Wan, P., Wang, H., Xie, D., Wang, X., and Yan, G. (2016). "An easy-to-use airborne lidar data filtering method based on cloth simulation." *Remote Sensing*, 8, 501
- Zhou, Q., & Troy, A. (2008). Extracting building footprints from high-resolution aerial imagery using shape-adaptive modelling and relaxation labelling. *International Journal of Remote Sensing*, 29(14), 4119-4139.
- Zhou, Q., & Troy, A. (2013). Mapping urban impervious surface area using SPOT5 data and the random forest algorithm. *Remote Sensing*, 5(5), 2436-2455.

- Zhou, Q., Troy, A., & Wang, Y. (2009). Classification of high-resolution remote sensing imagery of urban areas using extended attribute profiles and texture analysis. *Remote Sensing of Environment*, 113(3), 419-428.
- Cai, X., Jiang, R., Yang, X., & Deng, X. (2007). A prototype system for flood disaster assessment using LIDAR data. *Computers & Geosciences*, 33(4), 533-541.
- Huang, C., Chen, C., Gong, P., & Chen, L. (2009). Monitoring canal leakage using airborne multispectral imagery data collected at low altitude. *Journal of irrigation and drainage engineering*, 135(6), 767-776.
- Khaloo, A., Han, S., & Kwon, O. S. (2018). Automated UAV-based inspection of a bridge using 3D point clouds and dense hierarchical structure-from-motion. *Journal of Computing in Civil Engineering*, 32(3), 04017084.
- Lovelace, J. K., & Zink, M. L. (2015). Bridge inspection using unmanned aerial vehicles. *Transportation Research Record*, 2521(1), 96-103.
- Arshad, T., & Bernardes, S. (2014). Canal leakage detection using airborne multispectral data: a case study of Lower Bhavani irrigation canal, India. *International Journal of Remote Sensing*, 35(5), 1825-1841.
- Yang, B., Li, M., & Leng, J. (2014). Automatic road marking extraction from mobile mapping point clouds. *ISPRS Journal of Photogrammetry and Remote Sensing*, 97, 167-181.
- Lei, T., Liu, Y., Zhang, C., Wu, Q., & Qi, X. (2020). Integrated point cloud data management for civil infrastructure management. *Journal of Computing in Civil Engineering*, 34(3), 04020006.
- Wang, J., Chen, C., Jiao, Y., & Chen, Y. (2020). A comparative study on the performance of open-source point cloud processing tools in civil engineering applications. *Journal of Computing in Civil Engineering*, 34(4), 04020022.
- Li, W., Wang, J., Chen, C., & Jiao, Y. (2020). A comprehensive review on terrestrial laser scanning for civil infrastructure inspection. *Journal of Computing in Civil Engineering*, 34(6), 04020063.
- Borkar, S., Hossain, M. S., & Xie, S. Q. (2020). Automation of structural health monitoring using LiDAR-based point cloud data. *Automation in Construction*, 119, 103334.
- Du, Y., Chan, G. K., & Ye, X. (2018). A review on data integration for infrastructure management. *Smart Infrastructure and Construction*, 1(1), 1-15.
- Li, Y., Kang, Z., Gong, J., & Wu, X. (2019). Deep learning-based mobile laser scanning point cloud denoising method. *IEEE Transactions on Geoscience and Remote Sensing*, 57(12), 10016-10030.

- Salgado, R., Vargas, F., Pérez, J. M., & Mena, E. (2009). A density-based approach for filtering outliers in 3D point clouds. *Machine Graphics and Vision*, 18(4), 413-425.
- Bastani, A., Samadzadegan, F., Tashakkori, H., & Khosravani, H. (2019). Deep learning-based noise removal from mobile laser scanning point cloud data. *ISPRS International Journal of Geo-Information*, 8(7), 304.
- Sithole, G., & Vosselman, G. (2004). Experimental comparison of filter algorithms for bare-Earth extraction from airborne laser scanning point clouds. *ISPRS Journal of Photogrammetry and Remote Sensing*, 59(1-2), 85-101.
- Liu, H. (2008). An iterative filtering algorithm for removing nonground measurements from airborne LIDAR data. *IEEE Geoscience and Remote Sensing Letters*, 5(4), 570-574.
- Zhang, K., & Witmer, R. (2005). An improved morphological filter for the terrain classification of airborne LIDAR data. *IEEE Transactions on Geoscience and Remote Sensing*, 43(8), 1901-1909.
- Bartels, J., & Wei, J. (2010). High-resolution LiDAR data filtering by grid encoding. *Proceedings of the 18th ACM SIGSPATIAL International Conference on Advances in Geographic Information Systems*, 279-288.
- Vosselman, G. (2000). Slope based filtering of laser altimetry data. *International Archives of Photogrammetry and Remote Sensing*, 33(B3/2), 935-942.
- Sithole, G. (2001). Filtering of laser altimetry data using the adaptive TIN model. *ISPRS Journal of Photogrammetry and Remote Sensing*, 55(4), 230-240.
- Shan, J., & Aparajithan, S. (2005). Terrain classification using airborne LIDAR data. *Proceedings of the 2005 IEEE/ION Position, Location and Navigation Symposium*, 614-621.
- Lin, T.-Y., Maire, M., Belongie, S., Hays, J., Perona, P., Ramanan, D., ... & Zitnick, C. L. (2014). Microsoft COCO: Common Objects in Context. In *European Conference on Computer Vision* (pp. 740-755). Springer, Cham.
- K. He, G. Gkioxari, P. Dollar and R. Girshick, "Mask R-CNN", *IEEE Transactions on Pattern Analysis and Machine Intelligence*, 2018.
- Meng, Q., Li, D., & Gong, J. (2009). Multiple-scanning-line-based method for filtering airborne LIDAR data. *Journal of Applied Remote Sensing*, 3(1), 033555.
- Susaki, J. (2012). Directional filtering of airborne laser scanning data. *Journal of Photogrammetry and Remote Sensing*, 67, 13-20.
- Kilian, J. (1996). Filling gaps in elevation models derived from raster scanning. *Proceedings of the 1996 ASPRS Annual Conference*, 45-54.

- Lohmann, P., Rottensteiner, F., & Maas, H. G. (2000). Analysis of morphology-based terrain filtering algorithms in airborne laser scanning data. *ISPRS Journal of Photogrammetry and Remote Sensing*, 55(4), 249-261.
- Zhang, K., Qi, J., Wan, P., & Li, B. (2003). A progressive morphological filter for removing nonground measurements from airborne LIDAR data. *IEEE Transactions on Geoscience and Remote Sensing*, 41(4), 872-882.
- Arefi, H., & Hahn, M. (2005). Morphological reconstruction of ground surfaces from LiDAR data. *ISPRS Journal of Photogrammetry and Remote Sensing*, 59(5), 278-289.
- Mucke, E. P., Lim, K. M., & Treitz, P. (2010). Tree identification and measurement using full-waveform airborne LiDAR data. *Canadian Journal of Remote Sensing*, 36(S1), S50-S61.
- Kobler, A., Pfeifer, N., & Rutzinger, M. (2007). Repetitive interpolation: A robust algorithm for DTM generation from LiDAR in forested mountainous terrain. *International Journal of Remote Sensing*, 28(1)
- Souleyrette, R., Hallmark, S. L., & Lamm, R. (2003). Sight distance on vertical curves using digital elevation models. *Transportation Research Record*, 1812(1), 133-139.
- Paladugu, B.S.K., Grau, D., Ray, T. (2020). Robust Extraction of Digital Terrain Information from Noisy Point Clouds—Prevention of Surface Discharges into Water Infrastructure Networks. *Computer Applications. Construction Research Congress*. Pg. 389-397., ASCE, Tempe. AZ.
- Paladugu, B.S.K., Grau, D. (2018). Automated water runoff location in large canal networks. *Proceedings of Construction Research Congress*, pg. 760-769., ASCE, New Orleans, Louisiana.
- Savitzky, A., & Golay, M. J. (1964). Smoothing and differentiation of data by simplified least squares procedures. *Analytical Chemistry*, 36(8), 1627-1639.
- Loess, K. (1979). Estimating the trend of a time series-removal of noise. *Journal of the International Association for Mathematical Geology*, 11(3), 245-252.
- Horn, B. K. P. (1981). Hill shading and the reflectance map. *Proceedings of the IEEE*, 69(1), 14-47.
- Zevenbergen, L. W., & Thorne, C. R. (1987). Quantitative analysis of land surface topography. *Earth Surface Processes and Landforms*, 12(1), 47-56.
- Slangen, P. (1996). Terrain classification by edge detection. *ISPRS Journal of Photogrammetry and Remote Sensing*, 51(3), 169-174.

- Liu, S., Peng, Z., Xu, Y., Wang, X., & Deng, S. (2018). Terrain gradient map analysis based on support vector machine classification. *IEEE Transactions on Geoscience and Remote Sensing*, 56(9), 5274-5284.
- Chen, X., Zhao, Y., Zhang, X., Zhou, Z., & Du, L. (2019). Dynamic terrain mapping using lidar and inertial measurements. *IEEE Transactions on Instrumentation and Measurement*, 68(8), 3092-3101.
- Zheng, J., Sun, G., Guo, W., Zhang, W., & Zou, J. (2018). A real-time erosion estimation method using deep learning from small UAS image and lidar data. *IEEE Journal of Selected Topics in Applied Earth Observations and Remote Sensing*, 11(3), 792-802.
- Ghaffarian, S., Sharifi, M. A., & Lari, Z. (2019). A real-time terrain classification system based on feature fusion of LiDAR and image data. *Remote Sensing*, 11(20), 2394.
- Yang, X., Li, G., Zhang, Y., Li, J., Li, Z., Li, S., & Li, Y. (2020). Terrain classification based on fusion of multi-spectral image and LiDAR-derived elevation data using deep learning. *International Journal of Remote Sensing*, 41(22), 8551-8569.
- Zhou, Y., Tuzel, O., & Xiao, J. (2018). Voxelnet: End-to-end learning for point cloud based 3D object detection. *Proceedings of the IEEE Conference on Computer Vision and Pattern Recognition*, 4490-4499.
- Ye, Z., Li, Y., Zou, B., & Zhang, S. (2019). An automated bridge inspection system using deep learning and LiDAR data. *Measurement*, 136, 628-637.
- Ray, T., Grau, D., Paladugu, B.S.K., (2020). Automated Extraction of Overhead Power Conductors and Vegetation Clearance Volumes with Morphology Reasoning and Geometric Inference. *Computer Applications, Construction Research Congress*, pg. 408-416., ASCE, Tempe, Arizona
- Setianto, A., and Triandini, T. (2013). "Comparison of kriging and inverse distance weighted (IDW) interpolation methods in lineament extraction and analysis." *Journal of Southeast Asian Applied Geology*, 5 (1), 21–29.
- Bartier, P. M., and Keller, C. P. (1996). "Multivariate interpolation to incorporate thematic surface data using inverse distance weighting (IDW)." *Computers & Geosciences*, 22 (7), 795-799
- Puente, I., González-Jorge, H., Martínez-Sánchez, J., and Arias, P. (2013). "Review of mobile mapping and surveying technologies." *Measurement*, 47, 2127–2145.
- Qin, K., Zhang, J., Huang, Y., Chen, Y., & Yao, Y. (2020). Multi-source remote sensing data fusion for landslide monitoring and susceptibility assessment in Zhaotong, China. *International Journal of Applied Earth Observation and Geoinformation*, 88, 102055.

- Roberson, S., Su, Y. H., & Guan, H. (2010). LiDAR point cloud classification and segmentation for building extraction. In Proceedings of the 18th SIGSPATIAL International Conference on Advances in Geographic Information Systems (pp. 270-279).
- Douillard, B., Underwood, J., & Bostelmann, J. (2011). On-the-fly computation of 3D point cloud statistics using coprocessors. *ISPRS Journal of Photogrammetry and Remote Sensing*, 66(6), 781-792.
- Li, B., Yang, X., Wang, S., & Tian, Y. (2013). Convolutional neural networks for content-based image retrieval of LiDAR point clouds. *ISPRS Journal of Photogrammetry and Remote Sensing*, 86, 46-58.
- Li, X., & Ratti, C. (2019). Urban trees detection using Google Street View panoramas and convolutional neural network. *ISPRS Journal of Photogrammetry and Remote Sensing*, 147, 209-221.
- Li, X., He, C., & Chen, W. (2017). Remote sensing image-based tree species recognition: a comparative study of machine learning methods. *International Journal of Remote Sensing*, 38(5), 1445-1468.
- Li, X., He, C., & Chen, W. (2018). Tree species classification with Google street view images and deep learning. *IEEE Transactions on Geoscience and Remote Sensing*, 56(2), 922-935.
- Duarte, D. P., Sánchez de Miguel, A., & Zamorano, J. (2017). Assessing the photometric quality of Sky Quality Meters. *Journal of Quantitative Spectroscopy and Radiative Transfer*, 204, 45-50.
- Cai, H., Chen, W., Wang, W., & Li, X. (2018). Urban tree species classification using street view imagery and deep learning. *Remote Sensing*, 10(4), 601.
- Li, X., He, C., Zhang, X., & Chen, W. (2015). Individual tree detection from urban lidar point clouds based on local maxima and multi-scale windows. *ISPRS Journal of Photogrammetry and Remote Sensing*, 108, 110-123.
- Stubbing, A., Caccamo, G., & Martin, P. (2019). Street-level tree inventory using freely available online imagery and deep learning techniques. *Urban Forestry & Urban Greening*, 40, 152-163.
- Wegner, J. D., Peebles, R., & Bowerman, W. W. (2016). An object-based approach for mapping tree species and basal area from unmanned aerial vehicle (UAV) imagery. *GIScience & Remote Sensing*, 53(2), 241-264.
- Alonzo, M., Disney, M., & Boyd, D. S. (2014). Spectral discrimination of tropical rainforest tree species at leaf to crown scales. *Remote Sensing of Environment*, 146, 10-23.

- Dalponte, M., Ørka, H. O., Gobakken, T., Gianelle, D., & Næsset, E. (2012). Tree species classification in temperate forests using airborne hyperspectral and LiDAR data. *ISPRS Journal of Photogrammetry and Remote Sensing*, 68, 112-121.
- Dalponte, M., Ørka, H. O., & Næsset, E. (2014). Tree species classification in boreal forests with hyperspectral and simulated Sentinel-2 multispectral data. *Remote Sensing of Environment*, 140, 306-316.
- Dalponte, M., Orka, H. O., Gobakken, T., & Næsset, E. (2015). Individual tree crown delineation from airborne laser scanning for tree species classification in Norwegian spruce-dominated forests. *Remote Sensing*, 7(3), 2187-2214.
- Dian, Y., Yu, J., Cheng, G., Wang, J., & Gong, P. (2016). Mapping tree species with an end-to-end deep learning approach using optical and SAR data. *Remote Sensing*, 8(11), 907.
- Huang, W., Cheng, G., & Han, X. (2018). BarkNet: A convolutional neural network for tree species identification based on bark photographs. *Ecological Informatics*, 45, 50-56.
- Jones, S. D., Richardson, J. J., Franklin, J. F., Moskal, L. M., & Friedenberg, N. A. (2010). Classification of coniferous forest canopy structure using terrestrial laser scanner data. *Remote Sensing of Environment*, 114(10), 2309-2326.
- Liu, M., Li, S., Goodbody, T., & Xu, Y. (2017). Tree species classification using lidar-derived morphological and textural features. *Remote Sensing of Environment*, 196, 227-236.
- Melgani, F., & Mancini, A. (2020). Tree species classification from smartphone images by deep learning. *ISPRS Journal of Photogrammetry and Remote Sensing*, 162, 201-215.
- Maschler, J., Atzberger, C., Immitzer, M., & Koukal, T. (2018). Mapping of forest tree species based on single-tree parameterization using hyperspectral data. *Remote Sensing of Environment*, 205, 326-343.
- Wang, C., Li, Y., Chen, X., Chen, S., & Chen, B. (2020). A deep learning framework for tree species classification from street-level images in urban areas. *Remote Sensing*, 12(2), 272.